Dynein light chain 1 and a spindle-associated adaptor promote dynein asymmetry and spindle orientation

Anja K. Dunsch,[1] Dean Hammond,[2] Jennifer Lloyd,[2] Lothar Schermelleh,[1] Ulrike Gruneberg,[1] and Francis A. Barr[1]

[1]Department of Biochemistry, University of Oxford, Oxford OX1 3QU, England, UK
[2]Cancer Research Centre, University of Liverpool, Liverpool L3 9TA, England, UK

The cytoplasmic dynein motor generates pulling forces to center and orient the mitotic spindle within the cell. During this positioning process, dynein oscillates from one pole of the cell cortex to the other but only accumulates at the pole farthest from the spindle. Here, we show that dynein light chain 1 (DYNLL1) is required for this asymmetric cortical localization of dynein and has a specific function defining spindle orientation. DYNLL1 interacted with a spindle-microtubule–associated adaptor formed by CHICA and HMMR via TQT motifs in CHICA. In cells depleted of CHICA or HMMR, the mitotic spindle failed to orient correctly in relation to the growth surface. Furthermore, CHICA TQT motif mutants localized to the mitotic spindle but failed to recruit DYNLL1 to spindle microtubules and did not correct the spindle orientation or dynein localization defects. These findings support a model where DYNLL1 and CHICA-HMMR form part of the regulatory system feeding back spindle position to dynein at the cell cortex.

Introduction

Cytoplasmic dynein is a multisubunit force-generating AAA ATPase, or motor protein, with diverse cellular functions in both dividing and nondividing cells (Kardon and Vale, 2009). It has a complex structure comprised of a large, >400-kD heavy chain containing the ATPase domains, and a series of smaller subunits referred to as the light-intermediate, intermediate, and light chains, all associated with the N-terminal tail region of the heavy chain (Kardon and Vale, 2009). There are three different light chain (LC) subunits, LC7, LC8, and the T-complex testis-specific protein 1 (Kardon and Vale, 2009). A series of additional factors interact with dynein via these light and intermediate chains, the best characterized of which is dynactin, a multisubunit microtubule plus end–binding complex (Kardon and Vale, 2009). Dynactin acts in concert with other microtubule-associated proteins such as CLIP170, NudE, and EB1 to mediate the interaction of specific cargo with dynein at the microtubule (Kardon and Vale, 2009). Dynein can then promote the directed movement of the cargo toward the minus end of the microtubule.

In mitosis, dynein is found associated with specific regions of the cell cortex, as well as the mitotic spindle poles, spindle microtubules, and kinetochores (Pfarr et al., 1990; Steuer et al., 1990; Busson et al., 1998). Accordingly, disrupting dynein function results in defective and abnormally positioned or rotated spindles with misaligned chromosomes (Li et al., 1993; Echeverri et al., 1996; Gönczy et al., 1999; O'Connell and Wang, 2000; Sharp et al., 2000; Rebollo et al., 2007). Other evidence suggests that specific combinations of dynein adaptor proteins can independently regulate these functions. At the kinetochore, dynactin together with the Rod–ZW10–Zwilch complex, Lis1, Spindly, and NudE promotes microtubule attachment to the kinetochore, and also plays a role in mitotic checkpoint function (Starr et al., 1998; Scaërou et al., 1999; Faulkner et al., 2000; Wojcik et al., 2001; Williams et al., 2003; Cockell et al., 2004; Stehman et al., 2007; Chan et al., 2009; Gassmann et al., 2010).

Dynein is crucial for the exact positioning and rotation of the mitotic spindle in relation to extracellular cues in symmetric and asymmetric cell divisions during development (Rhyu and Knoblich, 1995; Kaltschmidt et al., 2000; Cabernard and Doe, 2009; Siller and Doe, 2009; Poulson and Lechler, 2010; Morin and Bellaïche, 2011). In part this is due to a role for dynein in a signaling pathway that relays information from a G protein–signaling module at the cell cortex to the spindle pole proteins NuMA and Aurora A in polarized cell divisions (Sanada and

D. Hammond and J. Lloyd contributed equally to this paper.
Correspondence to Francis A. Barr: francis.barr@bioch.ox.ac.uk
Abbreviation used in this paper: DYNLL1: dynein light chain 1.

© 2012 Dunsch et al. This article is distributed under the terms of an Attribution–Noncommercial–Share Alike–No Mirror Sites license for the first six months after the publication date (see http://www.rupress.org/terms). After six months it is available under a Creative Commons License (Attribution–Noncommercial–Share Alike 3.0 Unported license, as described at http://creativecommons.org/licenses/by-nc-sa/3.0/).

The Rockefeller University Press $30.00
J. Cell Biol. Vol. 198 No. 6 1039–1054
www.jcb.org/cgi/doi/10.1083/jcb.201202112

THE JOURNAL OF CELL BIOLOGY

Downloaded from http://rupress.org/jcb/article-pdf/198/6/1039/1575829/jcb_201202112.pdf by guest on 09 February 2026

Tsai, 2005; Bowman et al., 2006; Siller et al., 2006; Nguyen-Ngoc et al., 2007; Johnston et al., 2009; van der Voet et al., 2009; Zheng et al., 2010; Ellefson and McNally, 2011; Kiyomitsu and Cheeseman, 2012). NuMA together with dynactin is required for targeting of dynein to the cell cortex (Johnston et al., 2009; van der Voet et al., 2009; Woodard et al., 2010; Kiyomitsu and Cheeseman, 2012). Even so-called nonpolarized cells in culture typically position the mitotic spindle such that the axis of chromosome segregation is parallel to the growth surface (Toyoshima et al., 2007; Mitsushima et al., 2009). In this case, dynein–dynactin complexes play a role in the cortical capture and sliding of astral microtubules used to position and orient the spindle (Samora et al., 2011). Emerging evidence also implicates the retraction fibers, remnants of interphase cell–substratum adhesions, in spindle positioning and orientation in classical two-dimensional cell culture models (Théry et al., 2005; Fink et al., 2011). This may reflect the role of adhesion signaling through Rho family GTPases in more physiological cell divisions in tissues and three-dimensional cell culture systems (Gotta et al., 2001; Fernández-Miñán et al., 2007; Toyoshima et al., 2007; Buttrick et al., 2008; Jaffe et al., 2008; Inaba et al., 2010; Qin et al., 2010; Rodriguez-Fraticelli et al., 2010). Although a full picture has yet to emerge, current evidence supports the idea that a combination of extrinsic and intrinsic signals imparts defined spindle position and orientation (Kiyomitsu and Cheeseman, 2012).

As already mentioned, dynein is required for multiple processes during the formation and positioning of the mitotic spindle. However, the molecular nature of the different dynein complexes involved in spindle formation, positioning, and orientation remains unclear. We have therefore investigated the role of a specific cytoplasmic dynein light chain of the LC8 family, and find that it is needed together with a spindle-associated complex of CHICA and HMMR for correct spindle orientation.

Results

Dynein light chain 1 interacts with a subset of mitotic spindle proteins

To understand the function of dynein–dynein light chain 1 (DYNLL1) complexes at the mitotic spindle, HeLa cells stably expressing GFP-DYNLL1 were created. Analysis of DYNLL1 complexes isolated from mitotic populations of these cells by SDS-PAGE and mass spectrometry revealed the presence of dynein heavy, intermediate, light-intermediate, and the specific DYNLL1 light chain (Fig. 1 A and Table S1). In addition to these dynein subunits, a subset of mitotic spindle proteins were identified. Two of these, astrin and kinastrin/SKAP, have previously been reported to form a complex that interacts with dynein–DYNLL1 (Schmidt et al., 2010; Dunsch et al., 2011). A further two, HMMR/RHAMM and CHICA/FAM83D, are novel components of DYNLL1 complexes (Maxwell et al., 2003; Evanko et al., 2004; Santamaria et al., 2008; Tolg et al., 2010). Western blotting confirmed the presence of the different dynein subunits, astrin, kinastrin, HMMR, and CHICA in DYNLL1 complexes identified by mass spectrometry (Fig. 1 B). It also showed that these complexes do not contain tubulin, or other

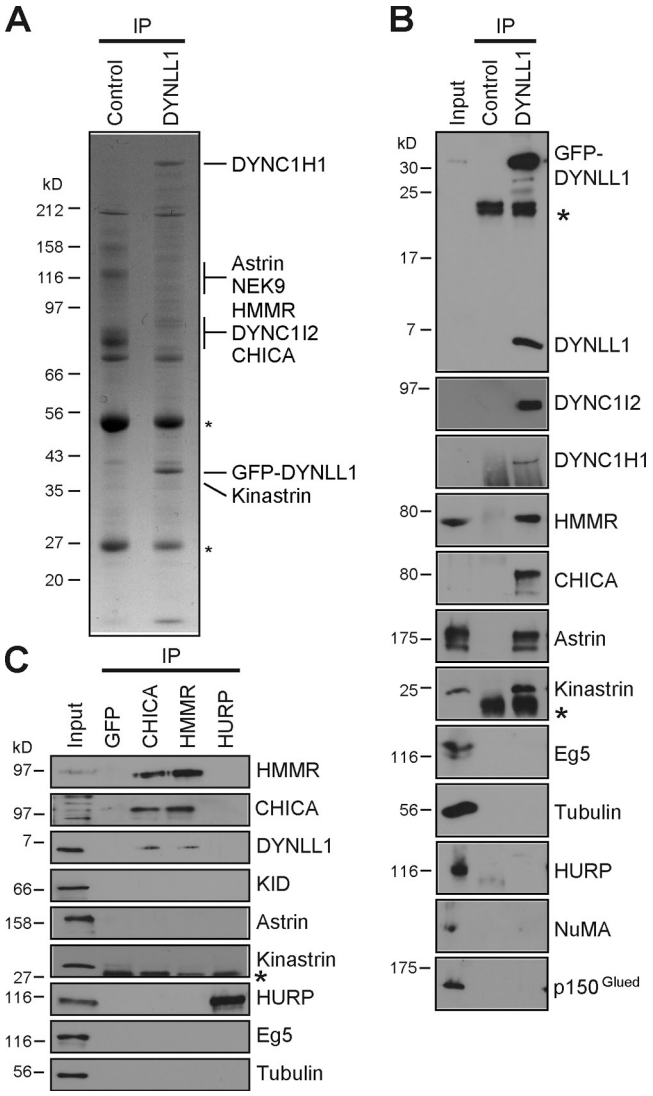

Figure 1. **DYNLL1-dynein associates with a defined subset of spindle proteins in mitosis.** (A) Control and DYNLL1 complexes were analyzed by SDS-PAGE and the major Coomassie blue–stained proteins identified by mass spectrometry are marked, or (B) by Western blotting using the specific antibodies shown in the figure. CHICA-C antibody was used for blotting. Asterisks mark the antibody heavy and light chains. (C) Complexes were immunoprecipitated using HMMR, CHICA-N, and HURP antibodies from HeLa cells arrested in mitosis using 200 ng/ml nocodazole for 18 h before cell lysis. Antibodies to GFP were used as a negative control. The immunoprecipitates were Western blotted using the antibodies shown in the figure. CHICA-C antibody was used for blotting. The asterisk marks light chain cross reactivity in the kinastrin blot.

spindle and spindle pole proteins Eg5, HURP, and NuMA, or the $p150^{Glued}$ subunit of dynactin. DYNLL1 therefore defines specific subcomplexes of dynein in mitotically arrested cells, which are discrete from those formed by dynactin.

Specific antibodies were then raised against HMMR and CHICA, and affinity purified to permit characterization of these two proteins and their interactions with DYNLL1. Western blotting showed that HMMR antibodies detected a single protein of the expected size, and that this was depleted by two different siRNA duplexes (Fig. S1 A). Similarly, CHICA antibodies detected a single protein of the expected size, and again this was depleted by two different siRNA duplexes (Fig. S1 A). These HMMR and

Downloaded from http://rupress.org/jcb/article-pdf/198/6/1039/1575829/jcb_201202112.pdf by guest on 09 February 2026

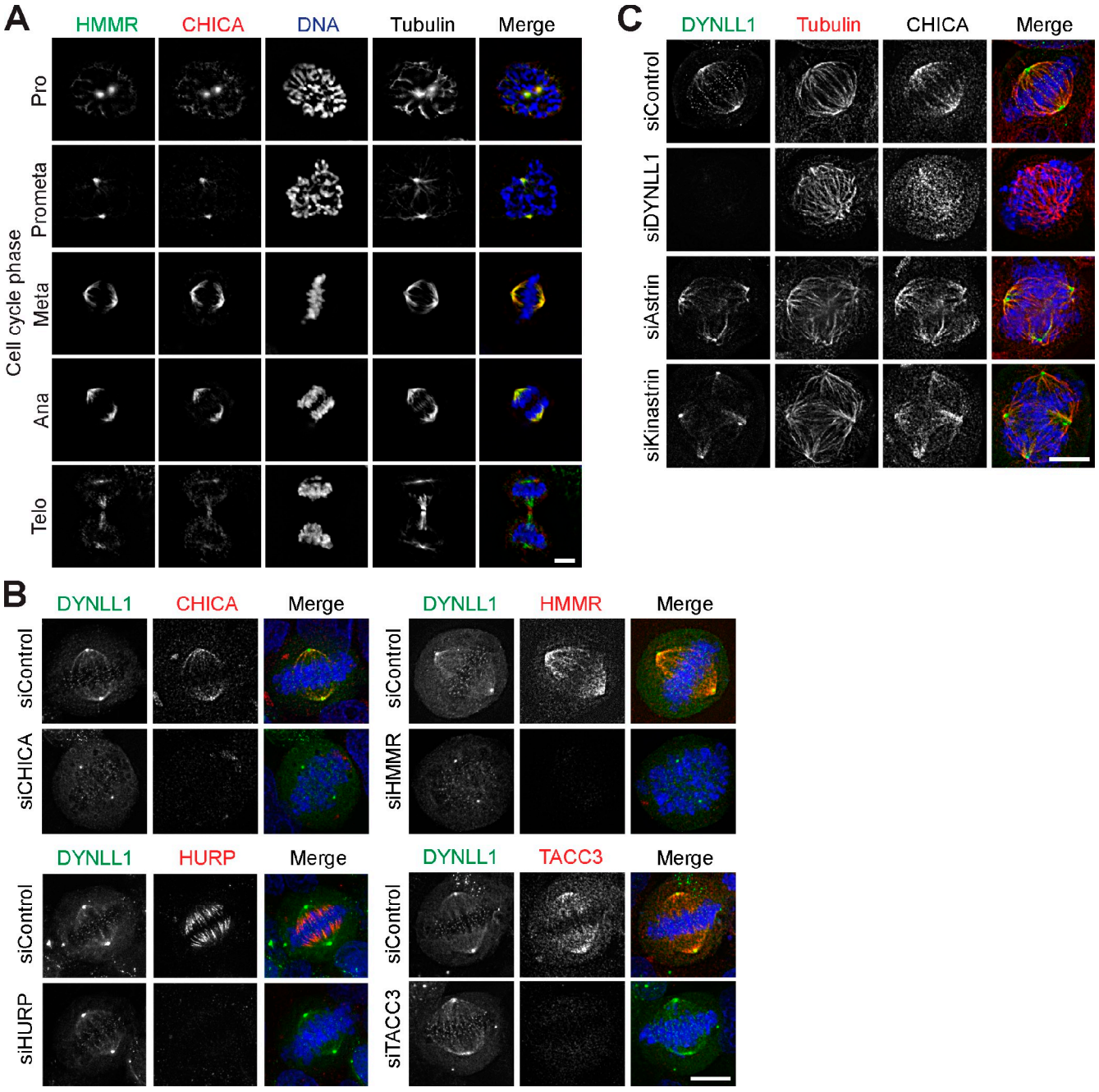

Figure 2. **HMMR and CHICA are spindle-associated factors required for DYNLL1 targeting.** (A) Asynchronous cultures of HeLa cells were fixed and then stained with mouse anti-HMMR, sheep anti-CHICA, rabbit anti-tubulin, and DAPI to detect DNA. Representative examples of the different stages of mitosis are shown. (B) HeLa cells stably expressing GFP-DYNLL1 were transfected with control, CHICA, HMMR, or HURP siRNA duplexes for 72 h, or TACC3 siRNA duplexes for 48 h. The cells were fixed and then stained for CHICA, HMMR, HURP, or TACC3 as appropriate and DAPI to detect DNA. DYNLL1 was visualized using GFP fluorescence. (C) HeLa cells stably expressing GFP-DYNLL1 were transfected with control, DYNLL1, or kinastrin, siRNA duplexes for 72 h, or astrin siRNA duplexes for 48 h. The cells were fixed and then stained for tubulin, CHICA, and DAPI to detect DNA. DYNLL1 was visualized using GFP fluorescence. CHICA-N antibodies were used for all stainings. Bars, 10 µm.

CHICA antibodies gave similar staining of the mitotic spindle, and in both cases this was lost in cells treated with specific siRNA duplexes. To test if HMMR and CHICA form a complex, these antibodies were used to immunoprecipitate the two proteins. Mass spectrometry (Table S1) and Western blotting (Fig. 1 C) revealed that CHICA and HMMR coprecipitate, consistent with the idea that the two proteins form a complex. In addition, DYNLL1 but not astrin or kinastrin were present in both CHICA and HMMR immunoprecipitates (Fig. 1 C). CHICA, HMMR, and DYNLL1 were not present in control or immunoprecipitations of the spindle and kinetochore fiber protein HURP (Fig. 1 C).

Spindle targeting of DYNLL1 requires HMMR and CHICA

The localization of HMMR and CHICA as cells passed through mitosis was then investigated (Fig. 2 A). This revealed that both

Downloaded from http://rupress.org/jcb/article-pdf/198/6/1039/1575829/jcb_201202112.pdf by guest on 09 February 2026

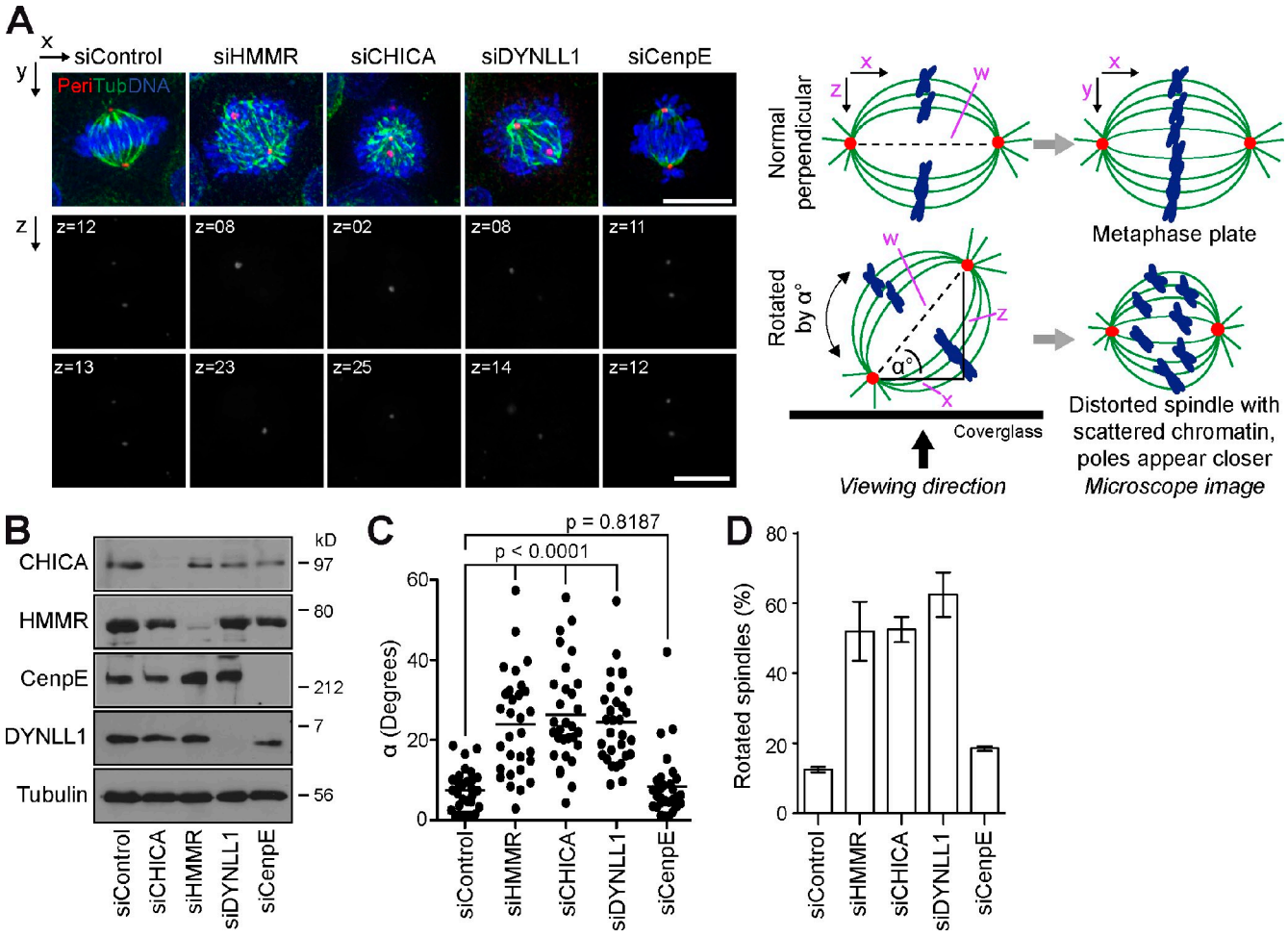

Figure 3. **Spindle orientation is perturbed in CHICA-, HMMR-, and DYNLL1-depleted cells.** (A) HeLa cells were transfected with control, CHICA, HMMR, DYNLL1 siRNA duplexes for 72 h, or CenpE siRNA duplexes for 48 h. The cells were fixed and then stained for tubulin and pericentrin to define the position of the mitotic spindle, and DAPI to detect DNA. A schematic shows the distances x and z measured from the microscope images and used to calculate α, the angle of spindle rotation and w, the pole-to-pole distance. (B) Samples were Western blotted to test for depletion of the respective target proteins. CHICA-C antibody was used for blotting. (C) Plots showing the angle of spindle rotation for cells depleted of the proteins indicated in the figure (n = 30). The Mann-Whitney test was used to calculate P-values for comparison of control and experimental samples. Median spindle angle was significantly different ($P < 0.0001$) in the DYNLL1-, HMMR-, and CHICA-depleted cells but not the CenpE-depleted cells ($P = 0.8187$) when compared with the control. (D) The percentage of cells with rotated spindles is plotted in the graph, error bars show the SEM (n = 100 in three independent experiments).

proteins localize to the spindle poles in prophase and prometaphase, and then spread out along the mitotic spindle in metaphase and then dissociate from the spindle in anaphase and telophase (Fig. 2 A). Depletion of either HMMR or CHICA, but not two other spindle proteins HURP or TACC3, resulted in a reduction of DYNLL1 at the mitotic spindle (Fig. 2 B). By contrast, depletion of the other DYNLL1-associated proteins astrin or kinastrin did not result in the loss of DYNLL1 from the spindles (Fig. 2 C), although spindles were highly disorganized as expected (Schmidt et al., 2010; Dunsch et al., 2011). Careful examination of astrin- and kinastrin-depleted cells revealed that DYNLL1 was lost from kinetochores, consistent with previous findings (Schmidt et al., 2010). Together, these findings show that DYNLL1 is present in two discrete complexes at the mitotic spindle: one containing astrin and kinastrin, the second previously uncharacterized complex containing HMMR and CHICA. The function of this latter complex and its relationship to dynein–DYNLL1 was therefore investigated further.

HMMR, CHICA, and DYNLL1 are required for normal mitotic progression

Previous studies have suggested that XRHAMM, the *Xenopus* orthologue of HMMR, has a function in the centrosome-independent pathway of spindle assembly (Groen et al., 2004). Other work suggests that HMMR promotes microtubule instability in interphase cells, and is important for mitotic spindle integrity (Tolg et al., 2010). By contrast, CHICA has been linked to the targeting of the kinesin-like motor protein KID to the mitotic spindle (Santamaria et al., 2008). HeLa cells were therefore depleted of HMMR, CHICA, or DYNLL1. Examination of these cells revealed apparently abnormal spindles with scattered chromatin (Fig. S1 B). A slight increase in mitotic index relative to the control was also observed for all CHICA, HMMR, and DYNLL1 duplexes tested (Fig. S1 C), consistent with the idea they have a function in mitosis. Live-cell imaging of cells expressing GFP-tubulin and mCherry-histone H2B showed that depletion of HMMR, CHICA, or DYNLL1 resulted

Downloaded from http://rupress.org/jcb/article-pdf/198/6/1039/1575829/jcb_201202112.pdf by guest on 09 February 2026

in an increase in the time taken from nuclear envelope breakdown (NEBD) to the onset of anaphase from 70 min in control cells to 110 min (Fig. S1 D). Although chromosomes and microtubules appeared disordered during spindle formation in each of these conditions, there was no obvious effect on chromosome segregation in anaphase (unpublished data). Other possibilities were that either kinetochore fiber function or spindle checkpoint activation were altered in the absence of the HMMR–CHICA–DYNLL1 complex. Speaking against these, cold-stable kinetochore fibers were still present in HMMR-, CHICA-, and DYNLL1-depleted cells, (Fig. S2 A), and none of these proteins localize to kinetochore fibers (Fig. S2 B). Furthermore, HMMR- and CHICA-depleted cells showed the expected localizations of the Bub1 checkpoint protein (Fig. S2 C) and a robust arrest in response to nocodazole (Fig. S2 D). These findings show that the HMMR–CHICA–DYNLL1 complex is not essential for kinetochore fiber stabilization or activation of the spindle checkpoint pathway. The role of DYNLL1 and the CHICA–HMMR complex in other dynein-dependent mitotic events was therefore investigated.

HMMR, CHICA, and DYNLL1 are required to define spindle orientation

In standard microscopy, cells are viewed through a coverglass that also acts as the growth surface, and a series of images collected at different focal positions through the sample data are projected to give a 2D image of the 3D sample (Fig. 3 A, schematic). Because cells grown in this way typically align the mitotic spindle parallel to the glass surface, this gives rise to the characteristic bar-like array of chromosomes (Fig. 3 A). Both spindle poles, defined in this case by the centriolar marker pericentrin are therefore typically equidistant from the coverglass or growth surface. This results in spindles aligning to within 10° of the plane of the coverglass. However, in cells depleted of HMMR, CHICA, or DYNLL1 (Fig. 3 B), the spindle poles are found at different distances from the coverglass (Fig. 3 A), and spindles showed widely differing angles of 0–60° to the coverglass plane (Fig. 3 C). Up to 60% of HMMR-, CHICA-, or DYNLL1-depleted cells had spindles rotated by over 10° (Fig. 3 D). These effects are not due to general perturbation of chromosome segregation because depletion of the CenpE motor protein required for proper chromosome alignment causes scattered chromatin but has little effect on spindle orientation compared with the control (Fig. 3, A–D).

Live-cell imaging was then performed to confirm these findings. As expected, cells depleted of CHICA, HMMR, or DYNLL1 showed apparently abnormal spindles (Fig. 4 A; see also Videos 1–4). Contrary to initial impressions, when the viewpoint was rotated these apparently abnormal spindles are revealed to be bipolar structures with the chromosomes aligned at a metaphase plate similar to the control cells (Fig. 4 B and Video 5). If spindle orientation was random in the absence of HMMR, CHICA, or DYNLL1, then the maximum angle observed should be 90°. However, none of the measurements made on fixed-cell samples exceeded 60°. One possibility was that the angle of spindle rotation was underestimated in the fixed samples due to drying artifacts causing flattening of the sample. Measurements of spindle rotation and pole-to-pole distance made from live-cell imaging data showed that spindles in HMMR-, CHICA-, or DYNLL1-depleted cells are of similar size (Fig. 4 C) but do not align to the coverslip, and the maximum angle of rotation is close to 90° compared with 10° in control samples (Fig. 4 D). DYNLL1, CHICA, and HMMR therefore act in a pathway required for proper mitotic spindle orientation.

Spindles orient at a fixed but incorrect angle

Inspection of the live-cell imaging data revealed that the spindles adopt a fixed but incorrect orientation with respect to the growth surface when DYNLL1, CHICA, or HMMR are depleted, and do not tumble continuously. Measurements over time for three individual cells for each condition showed that the spindle angle is rapidly established after bipolar spindle formation (Fig. 5, dotted line marks the point where a bipolar spindle is formed). Strikingly, even in cells showing prolonged time in metaphase this angle is maintained, typically within 10°, until the onset of anaphase (Fig. 5, marked by a red circle). Once in anaphase the angle of the spindle tends to zero as the cells flatten along the growth surface as they divide. The observation that spindle orientation became fixed indicated that the spindle was still contacting the cortex, suggesting that astral microtubules were not grossly altered. To clarify this, we made use of super-resolution 3D structured illumination microscopy (3D-SIM) to image the entire volume of mitotic cells under different depletion conditions. Astral microtubule organization was similar in DYNLL1-, CHICA-, or HMMR-depleted cells and control cells (Fig. 6 A). Furthermore, disruption of astral microtubules using 6.25 ng/ml nocodazole resulted in rotated but mainly off-center spindles positioned close to the cell cortex (Fig. 6, B and C). Under these conditions spindles are smaller due to altered microtubule dynamics, but kinetochore fibers still capture and align the chromosomes (Fig. 6 B). This effect is different to the consequences of depleting DYNLL1, CHICA, or HMMR. In these instances spindles are rotated but typically remain centered within the cell (Fig. 6 C). The microtubule plus end–tracking protein EB1 was then used to measure the dynamics of astral microtubules. This revealed that astral microtubule growth rates are similar in control, DYNLL1-, CHICA-, or HMMR-depleted cells (Fig. 6 D; see also Videos 6–10), and are in the range of values reported previously (Dunsch et al., 2011). These observations support the idea that astral microtubules play two roles in spindle positioning. First, they are important for centering the spindle within the cells, and second, they are used to transmit force during spindle rotation. Low doses of nocodazole disrupt the astral microtubules and interfere with both functions. However, the data presented here show that the DYNLL1 pathway is not required for astral microtubule formation, is not a major regulator of astral microtubule growth, and is not part of the NuMA–Plk1 intrinsic spindle-positioning pathway. This therefore suggests that DYNLL1, CHICA, and HMMR function during spindle rotation rather than as direct regulators of astral microtubules.

Downloaded from http://rupress.org/jcb/article-pdf/198/6/1039/1575829/jcb_201202112.pdf by guest on 09 February 2026

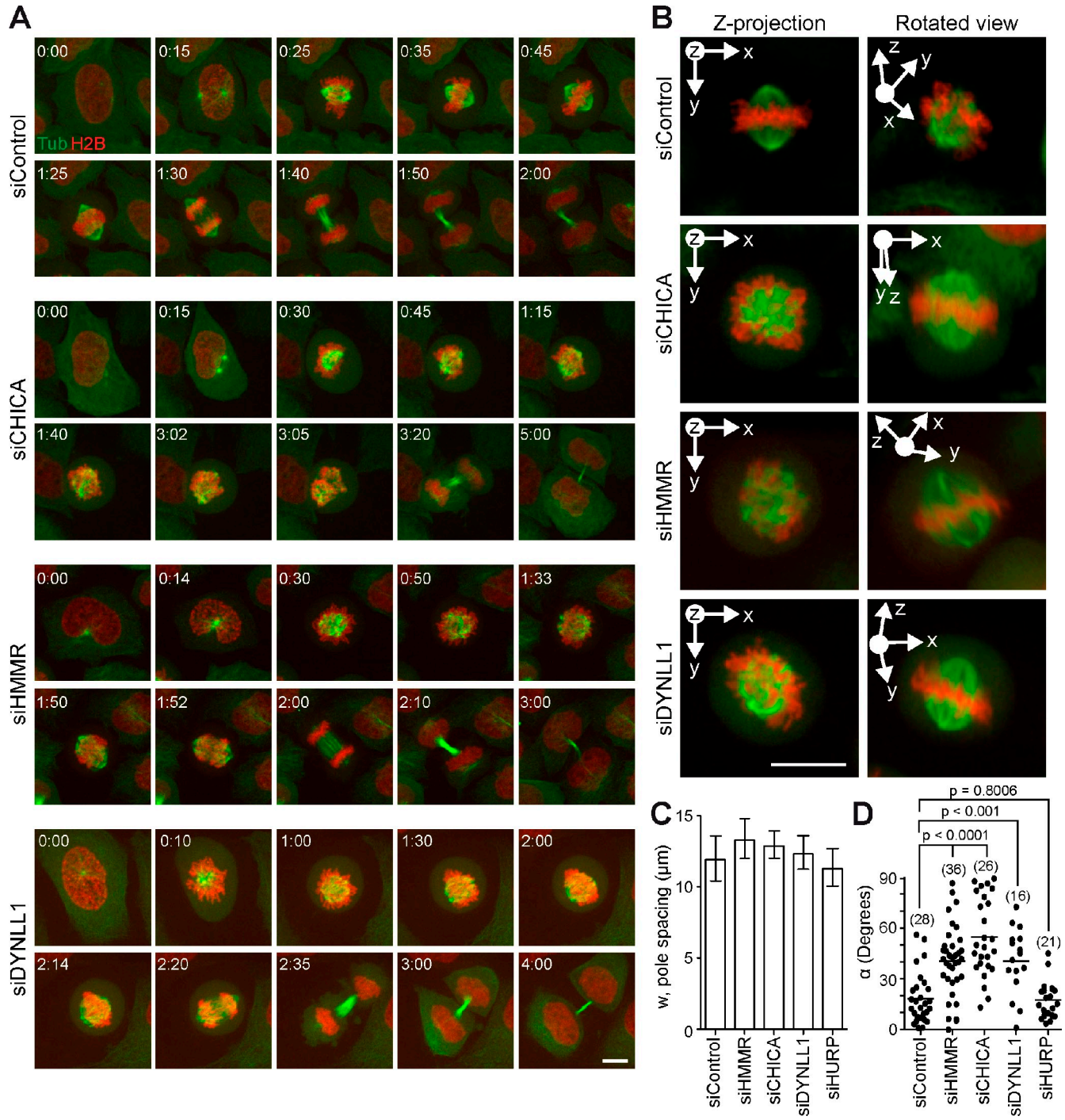

Figure 4. **HMMR, CHICA, and DYNLL1 are required for normal mitotic progression.** (A) HeLa cells stably expressing GFP-tubulin and mCherry-histone H2B were transfected with the siRNA duplexes shown in the figure for 72 h, and the full cell volume was imaged on an Ultraview spinning-disk confocal microscope every minute as the cells passed through mitosis. Maximum intensity projections of tubulin and histone H2B are shown at the times indicated in the figure. Bars, 10 µm. (B) A maximum intensity z-projection of tubulin and histone H2B are shown in the left column. The full 3D dataset was rotated to view the spindle from a plane perpendicular to the chromosomes and this is shown in the right column. (C) The pole-to-pole distance and (D) angle of spindle rotation at the metaphase-to-anaphase transition were calculated as described in Fig. 3 A and are plotted in the graphs. The Mann-Whitney test was used to calculate P-values for comparison of control and experimental samples. Median spindle angle was significantly different ($P < 0.0001$) in the HMMR- and CHICA-depleted cells, $P < 0.001$ in the DYNLL1-depleted cells, but not the HURP-depleted cells ($P = 0.8006$) when compared with the control. Numbers in brackets indicate sample size.

HMMR targets CHICA to the mitotic spindle

The functions of the different components of the HMMR–CHICA complex were then investigated to explain how it promotes proper spindle orientation. First, the localizations of a series of HMMR fragments were examined (Fig. 7 A). The first 189 amino acids of HMMR showed a strong spindle pole targeting in mitotic cells, and localized to microtubules in interphase cells

Downloaded from http://rupress.org/jcb/article-pdf/198/6/1039/1575829/jcb_201202112.pdf by guest on 09 February 2026

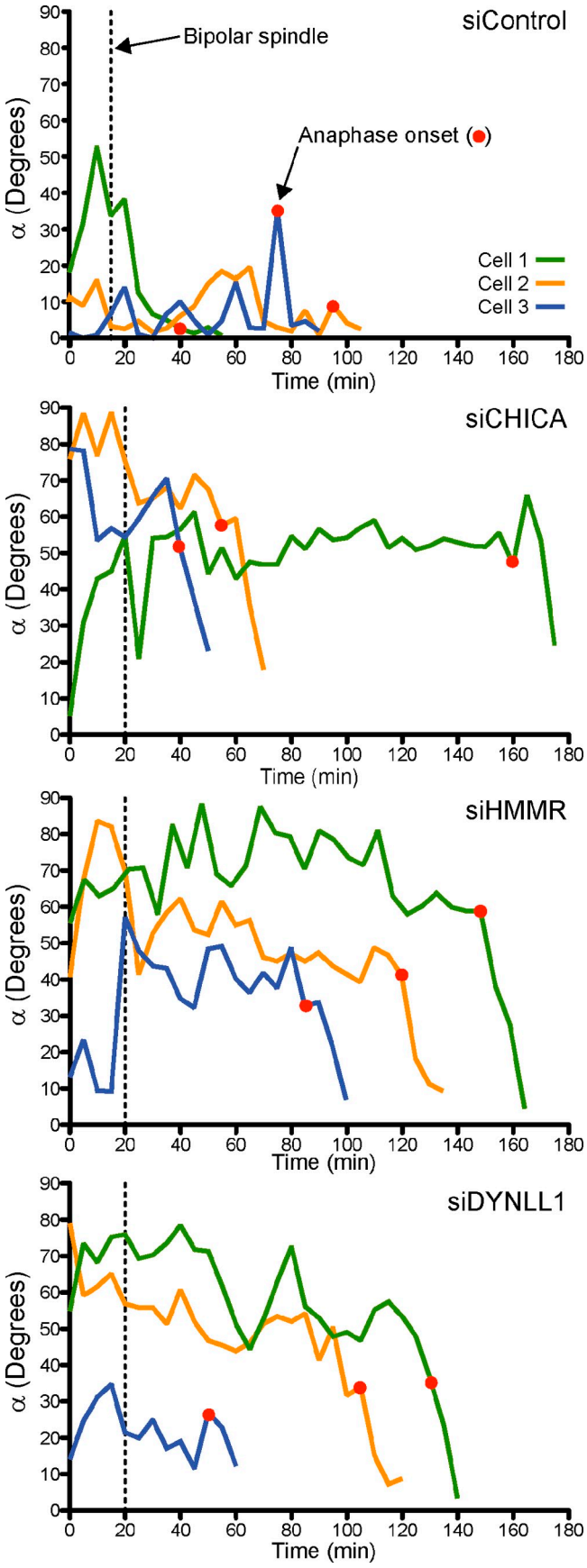

Figure 5. **Spindles adopt a fixed but incorrect orientation in CHICA-, HMMR-, or DYNLL1-depleted cells.** HeLa cells stably expressing GFP-tubulin and mCherry-histone H2B were transfected with the siRNA duplexes shown in the figure for 72 h, and the full cell volume was imaged on an Ultraview spinning-disk confocal microscope every minute as the cells passed through mitosis. The angle of spindle rotation was measured and is plotted in the graph as a function of time for three individual cells. The point at which bipolar spindle formation was complete is shown by the dotted line. A red circle marks the time point when chromosome segregation was first observed, taken as a marker for the onset of anaphase. Three example curves are shown taken from a single representative experiment of five replicates.

(Fig. 7 A). This fragment, but not the other fragments of HMMR, bound directly to microtubules when tested in in vitro pelleting assays (Fig. 7 B). A different region of HMMR, amino acids 365–546, within the predicted coiled-coil segment was required for binding to CHICA (Fig. 7 C). Reciprocal experiments with a series of CHICA fragments were then performed. This revealed that the C-terminal amino acids 383–615 localized to the mitotic spindle, and gave a weak microtubule staining in interphase cells (Fig. 7 D). However, this fragment did not show any microtubule-binding properties when tested in in vitro pelleting assays (Fig. 7 E). Mapping experiments revealed that the spindle-targeting fragment 383–615 was the binding site for HMMR (Fig. 7 F). The simplest explanation for these findings is that HMMR directly binds to microtubules and acts as an adaptor for CHICA, consistent with the requirement for HMMR in CHICA targeting to the spindle (Fig. S1 B).

Interaction of CHICA with DYNLL1 is required for spindle orientation

A series of elegant studies has identified a binding motif for the DYNLL1 protein defined by a highly conserved TQT sequence (Lo et al., 2001; Rapali et al., 2011a). Inspection of the CHICA sequence reveals the presence of three consensus TQT motifs (Fig. 8 A). Western blot analysis revealed that DYNLL1 was present in pulldowns of full-length CHICA or the 383–615 C-terminal fragment containing all three TQT motifs (Fig. 8 A). DYNLL1 was not detected in pulldowns of the other CHICA fragments tested. The three TQT motifs were then mutated to alanine, alone or in combination, to define their role in mediating the CHICA–DYNLL1 interaction. Mutation of all three TQT motifs in CHICA was necessary to abolish the interaction with DYNLL1 (Fig. 8 B). Furthermore, unlike the wild-type protein this triple TQT mutant was not able to target DYNLL1 to the spindle microtubules (Fig. 8 C), and did not correct the spindle orientation defect in CHICA-depleted cells (Fig. 8 D). DYNLL1 is therefore recruited to the mitotic spindle poles by a TQT motif–mediated interaction with CHICA, where it is required to establish the correct spindle orientation.

Asymmetric targeting of dynein to the cell cortex requires DYNLL1

During mitotic spindle positioning, dynein generates pulling forces to re-center and orient the mitotic spindle within the cell (Laan et al., 2012). In the course of this process, dynein oscillates from one pole of the cell cortex to the other but only accumulates at the pole farthest from the spindle (Kiyomitsu and Cheeseman, 2012). The cortical domains to which dynein localizes are defined by NuMA and other factors that do not show the

Downloaded from http://rupress.org/jcb/article-pdf/198/6/1039/1575829/jcb_201202112.pdf by guest on 09 February 2026

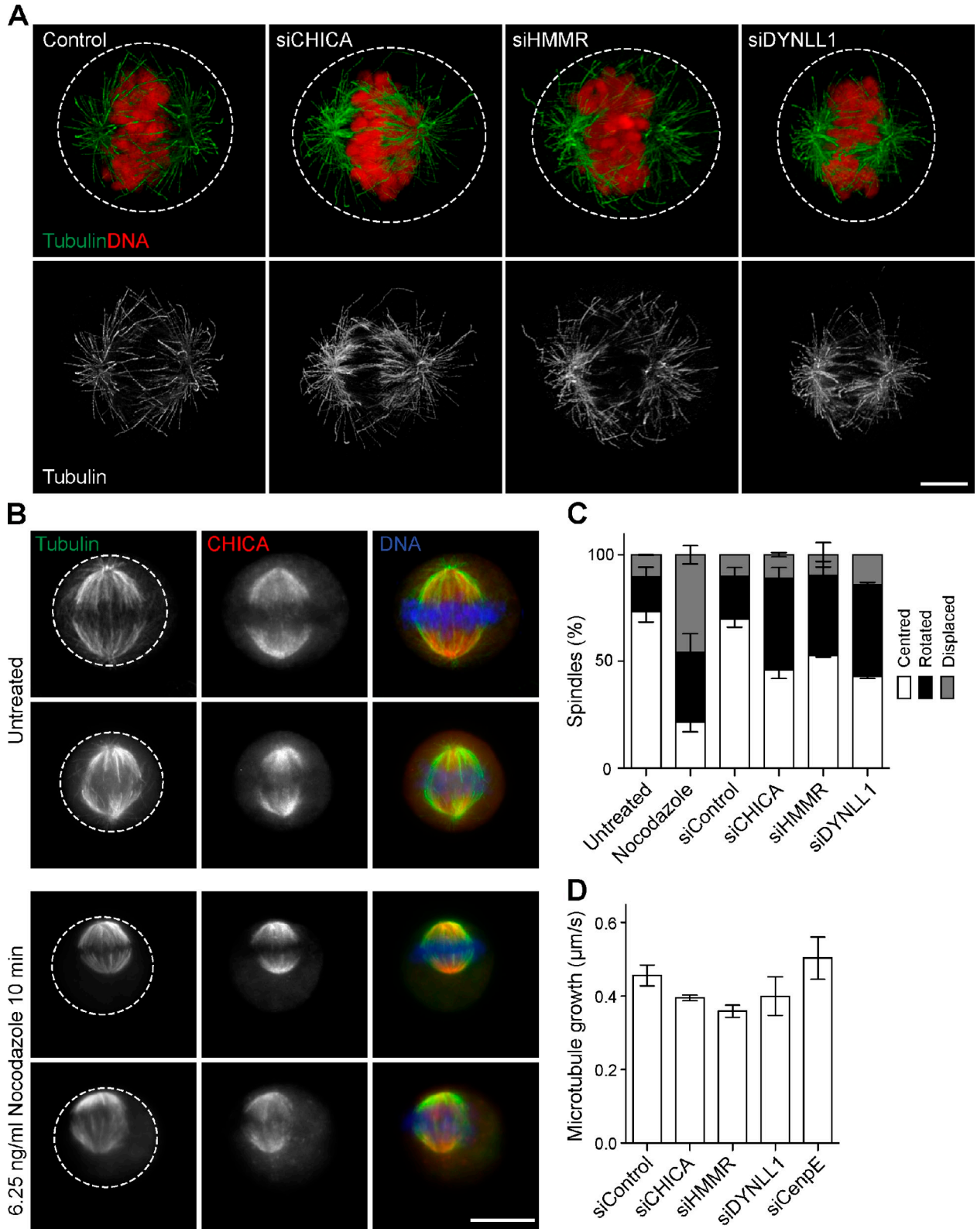

Figure 6. **Super-resolution imaging of astral microtubules in DYNLL1-, CHICA-, and HMMR-depleted cells.** (A) HeLa cells were transfected with control, HMMR, CHICA, or DYNLL1 siRNA duplexes for 72 h. The cells were fixed and then stained for CHICA, tubulin, and with DAPI to reveal DNA. Efficient depletion of CHICA and HMMR in these cells was confirmed by the loss of CHICA from the spindle microtubules (not depicted). Samples were analyzed by super-resolution imaging, and maximum intensity projections of the 3D-SIM stacks are shown from a viewpoint perpendicular to the pole-to-pole axis of the spindle. Bar, 5 µm. (B) To test the importance of astral microtubules in spindle positioning and rotation, HeLa cells were treated with a subcritical dose of nocodazole (6.25 ng/ml) for 10 min, fixed, and then stained for tubulin, CHICA, and with DAPI to reveal DNA. CHICA-C antibody was used for staining. Controls were left untreated. Example images are shown in the figure. Bar, 10 µm. (C) The number of cells with normally centered, rotated, or displaced spindles was counted and plotted in the graph. Error bars indicate the SEM (n = 50 in two independent experiments). (D) HeLa cells expressing

Downloaded from http://rupress.org/jcb/article-pdf/198/6/1039/1575829/jcb_201202112.pdf by guest on 09 February 2026

same oscillating behavior (Kiyomitsu and Cheeseman, 2012). To test if dynein function requires the DYNLL1–CHICA pathway, dynein localization was investigated using stable cell lines expressing GFP-tagged dynein heavy chain (DYNC1H1). In control cells, dynein was found asymmetrically localized to the cell cortex and to the mitotic spindle in 60% of cells (Fig. 9, A and B), as described previously (Kiyomitsu and Cheeseman, 2012). However, when DYNLL1, CHICA, or HMMR were depleted this asymmetric cortical localization was lost and dynein was found at both poles, or multiple smaller patches at the cell cortex (Fig. 9, A and B). Depletion of a kinetochore fiber protein HURP has no effect on dynein asymmetry at the cell cortex (Fig. 9, A and B). Although it was not possible to co-stain for dynein and NuMA, parallel experiments revealed that the underlying distribution of NuMA at the cell cortex was not altered by DYNLL1, CHICA, or HMMR depletion (Fig. S3). The additional dynein at the cell cortex may be relevant for the slightly increased pole-to-pole distance in these cells (Fig. 4, A and C), due to increased pulling forces on the two spindle poles. This may also delay satisfaction of the spindle assembly checkpoint due to alterations in spindle geometry, and therefore may explain the slight mitotic delays observed. Alternatively, it remains possible that DYNLL1 plays additional roles in the spindle checkpoint through other binding partners such as the astrin–kinastrin complex (Schmidt et al., 2010; Dunsch et al., 2011).

To show that the effect on dynein asymmetry is due to the pool of DYNLL1 interacting with the CHICA–HMMR complex at the mitotic spindle, rescue experiments using the CHICA TQT mutant defective in DYNLL1 binding were performed (Fig. 10). As described already, depletion of CHICA resulted in a loss of dynein asymmetry, and this could be rescued by expression of wild-type CHICA (Fig. 10, A and B). By contrast, the CHICA TQT mutant failed to support asymmetric dynein targeting to the cell cortex (Fig. 10, A and B). Together, these findings support the idea that the spindle-associated CHICA–HMMR complex acts as a regulator of dynein localization, and therefore its activity, through the DYNLL1 adaptor protein.

Discussion

A model for DYNLL1-CHICA function in spindle rotation

The findings presented here show that DYNLL1 and CHICA–HMMR form part of a regulatory system feeding back spindle position to dynein at the cell cortex. Based on this data, we propose a simple working model to explain the function of DYNLL1 and the CHICA–HMMR complex in spindle positioning (Fig. 10 C). CHICA and HMMR associate with the mitotic spindle through a spindle-microtubule–targeting region in the N terminus of HMMR. This complex can then recruit DYNLL1 via a series of canonical TQT motifs in the C-terminal region of CHICA. The model proposes that this will create a gradient of DYNLL1 activity, decreasing away from the spindle and spindle poles (Fig. 10 C, purple shaded region). During the formation of the mitotic spindle in prophase and prometaphase, or when a spindle is displaced away from the center of the cell, the spindle pole will approach the cell cortex. The resulting local increase in DYNLL1 then causes the loss of dynein from the cell cortex. This would explain why dynein can be isolated in complex with DYNLL1 and is found together with DYNLL1 at the mitotic spindle, but DYNLL1 does not localize to the cell cortex. When this inhibitory mechanism is lost, dynein localization becomes uncoupled from spindle rotation. Spindle position toward the center of the cell is relatively unaltered because astral microtubules will continue to push against the cell cortex and exert a centering effect. Providing independent support for this idea, pronounced oscillation of dynein localization and spindle position is only observed when astral microtubules are perturbed using nocodazole (Kiyomitsu and Cheeseman, 2012). A prediction of this model is that the DYNLL1-bound form of dynein cannot bind to dynein adaptors required for cortical targeting. Although not exhaustively tested, the biochemical and Western blot analysis of dynein–DYNLL1 complexes failed to reveal the presence of subunits of another major dynein adaptor dynactin or components such as NuMA required for cortical targeting of dynein.

DYNLL1-CHICA are components of the intrinsic spindle positioning pathway

Dynactin, together with NuMA and Lgn is required for targeting of dynein to the cell cortex (Johnston et al., 2009; van der Voet et al., 2009; Woodard et al., 2010; Kiyomitsu and Cheeseman, 2012). This system is controlled by extracellular cues (Théry et al., 2005, 2007; Toyoshima and Nishida, 2007; Siller and Doe, 2009), and signals intrinsic to the mitotic spindle (Kiyomitsu and Cheeseman, 2012). The spindle intrinsic signal has two components: one is the Ran-gradient system, the second is the spindle-associated mitotic kinase Plk1. Activated Ran in the vicinity of chromatin controls the interaction of importins with NuMA and modulates the interaction of the NuMA-Lgn complex with the membrane (Kiyomitsu and Cheeseman, 2012). Plk1 regulates the interaction of the NuMA-Lgn complex with dynein-dynactin, and therefore directly controls force generation (Kiyomitsu and Cheeseman, 2012). Together, these two components prevent dynein accumulation at the cell equator, and reduce dynein-dependent force generation at regions of the cell cortex close to the spindle poles. Further work will be needed to establish the relationship between these components and the DYNLL1-CHICA pathway. The most obvious possibility is that Plk1 regulates the DYNLL1-CHICA pathway through phosphorylation. Previous work has shown that CHICA is heavily phosphorylated in mitosis (Santamaria et al., 2008), but the

mCherry-tagged EB1 were transfected with control, HMMR, CHICA, or DYNLL1 siRNA duplexes for 72 h, or CenpE siRNA duplexes for 48 h. Cells were imaged at four planes positioned at the cell equator to cut through one or both spindle poles. Acquisition was with 30% laser power, 100-ms exposure time at maximum speed, equivalent to 0.87 frames per second. EB1 comets located between the spindle poles and the cell cortex, which mark growing astral microtubule ends, were identified and marked by eye in ImageJ and the mean distance moved per unit time calculated and plotted in the bar graph. Error bars indicate the SEM (n = 20).

Downloaded from http://rupress.org/jcb/article-pdf/198/6/1039/1575829/jcb_201202112.pdf by guest on 09 February 2026

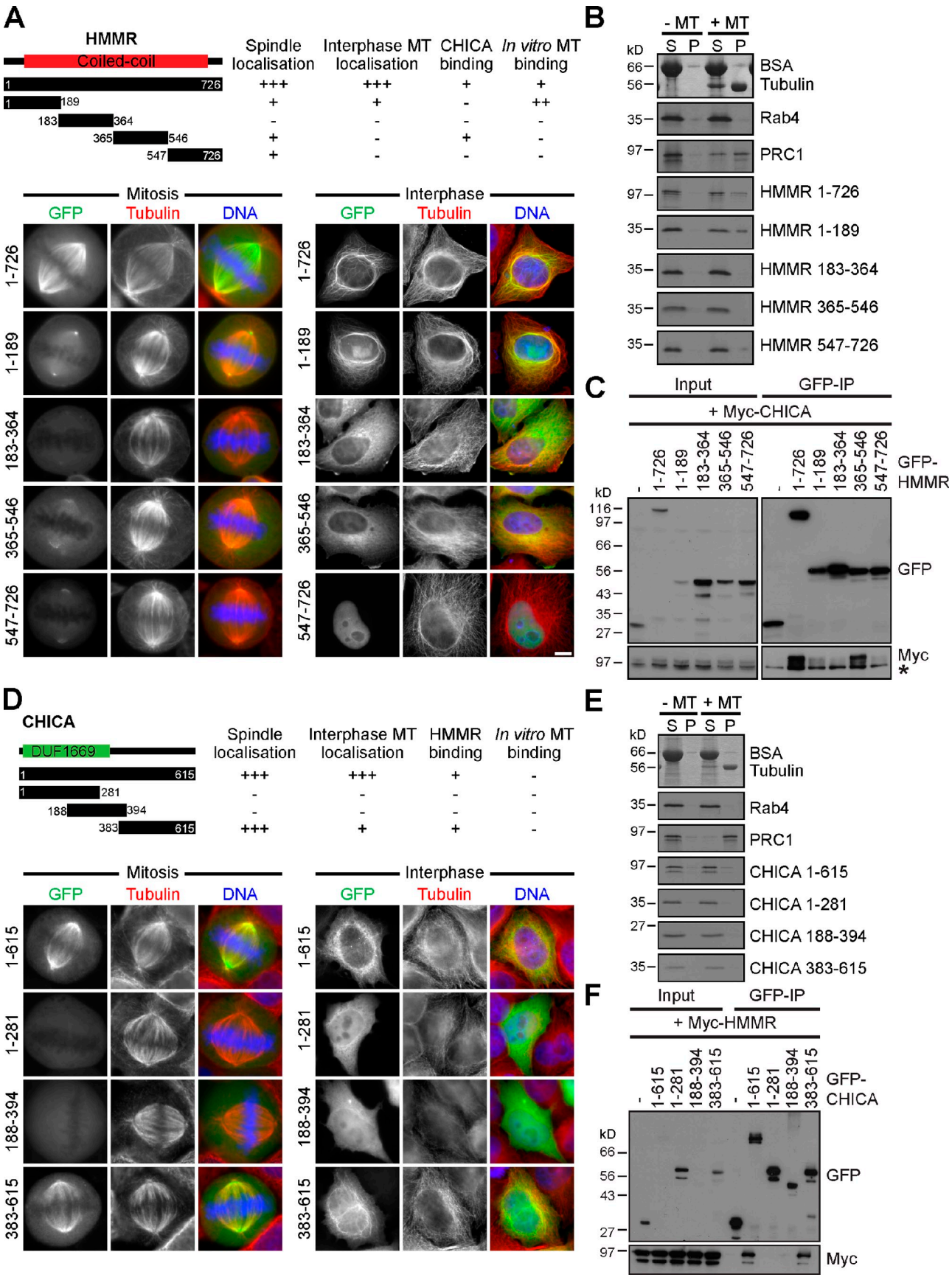

Figure 7. **HMMR is a microtubule-binding protein and partner of CHICA.** (A) HeLa cells were transfected with full-length GFP-tagged HMMR or the deletion constructs outlined in the schematic. After 24 h the cells were fixed and then stained for tubulin, and DAPI to detect DNA. HMMR was visualized using GFP fluorescence. Representative examples of the localization in mitotic or interphase cells are shown. Bar, 10 µm. (B) Microtubule-binding assays were

Downloaded from http://rupress.org/jcb/article-pdf/198/6/1039/1575829/jcb_201202112.pdf by guest on 09 February 2026

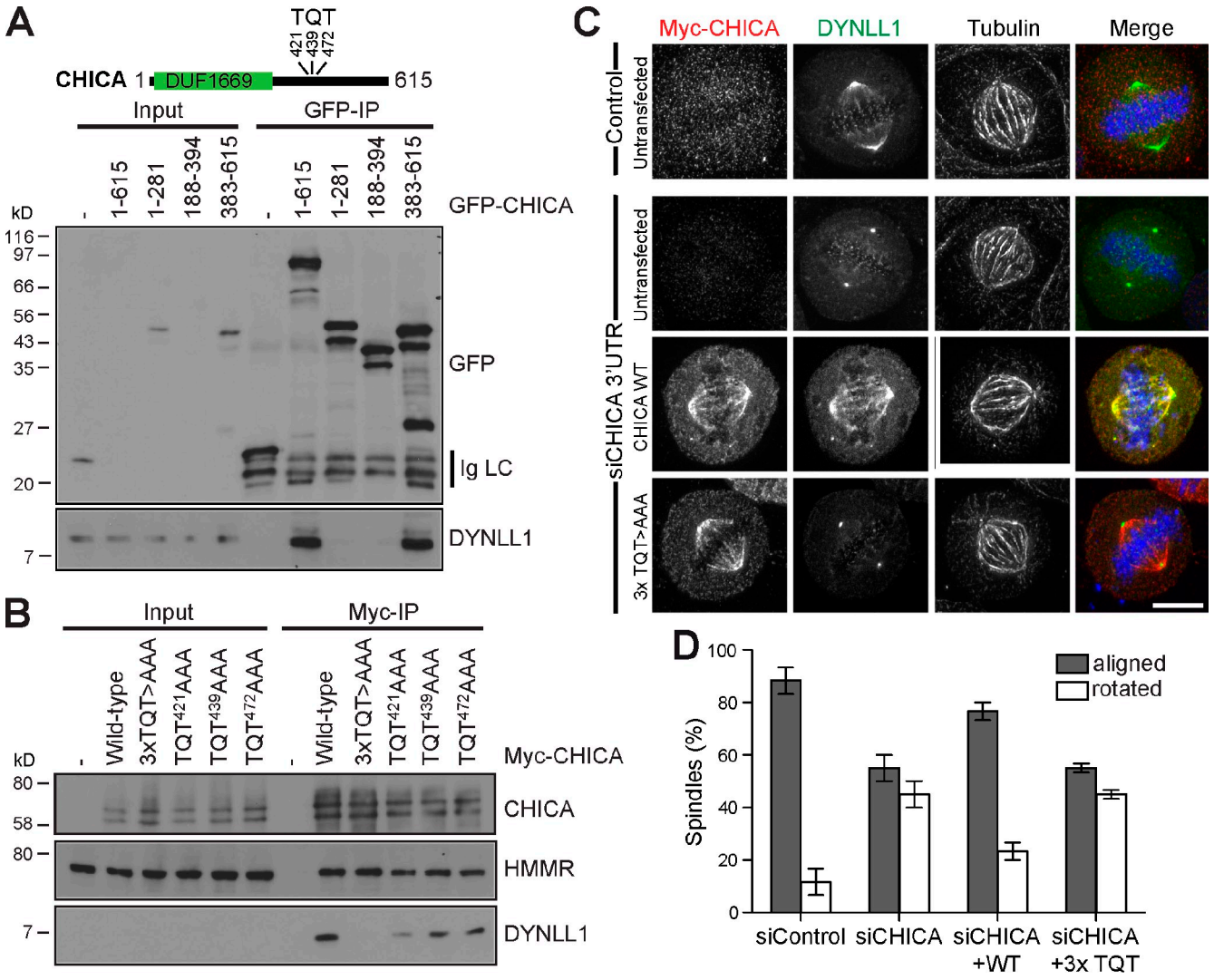

Figure 8. **CHICA binds to DYNLL1 via TQT consensus motifs.** (A) HEK293T cells were transfected with full-length and deletion constructs of GFP-CHICA for 30 h. CHICA complexes were immunoprecipitated using sheep anti-GFP antibodies, and then Western blotted using mouse anti-GFP or rabbit anti-DYNLL1 antibodies. (B) HEK293T cells were transfected with Myc-CHICA, and single or combined TQT to AAA mutants for 30 h. CHICA complexes were immunoprecipitated using mouse anti-Myc antibodies, and then Western blotted using rabbit anti-Myc, sheep anti-HMMR, or rabbit anti-DYNLL1 antibodies. (C) HeLa cells stably expressing GFP-DYNLL1 were treated with control siRNA or directed toward the 3′-UTR of CHICA for 72 h, and transfected with the wild-type or 3x TQT to AAA mutant forms of Myc-CHICA, fixed after 36 h, and then stained as indicated in the figure. DYNLL1 was directly visualized by GFP fluorescence. Bar, 10 µm. (D) The percentage of cells with aligned or rotated spindles is plotted in the bar graph. Error bars show the SEM (n = 30 in three experiments).

consequences of this modification remain unknown. Another area for future work will be the study of DYNLL1 interaction with dynein. This interaction is thought to be mediated by a TQT motif in the dynein intermediate chain (Rapali et al., 2011b), but the role this interaction plays in controlling dynein function and localization remains mysterious. Intriguingly, dynactin also binds to dynein via the dynein intermediate chain (Vaughan et al., 1995) and this interaction is mutually exclusive with another dynein regulator NudE-Lis1 (McKenney et al., 2011). Therefore, DYNLL1 may compete with dynactin for binding sites on the dynein intermediate chain, and thereby displace dynein complexes from the cell cortex.

performed using in vitro–translated full-length HMMR and the fragments shown in the figure. The anaphase spindle protein PRC1 and the small GTPase Rab4 were taken as positive and negative controls, respectively. (C) HEK293T cells were cotransfected with full-length and deletion constructs of GFP-HMMR and Myc-CHICA for 30 h. HMMR complexes were immunoprecipitated using sheep anti-GFP antibodies, and then Western blotted using mouse anti-GFP or mouse anti-Myc. An asterisk marks a nonspecific band in the Myc blots. (D) HeLa cells were transfected with full-length GFP-tagged CHICA or the deletion constructs outlined in the schematic. After 24 h, the cells were fixed and then stained for tubulin, and DAPI to detect DNA. CHICA was visualized using GFP fluorescence. Representative examples of the localization in mitotic or interphase cells are shown. Bar, 10 µm. (E) Microtubule-binding assays were performed using in vitro–translated full-length CHICA and the fragments shown in the figure. The anaphase spindle protein PRC1 and the small GTPase Rab4 were taken as positive and negative controls, respectively. (F) HEK293T cells were cotransfected with full-length and deletion constructs of GFP-CHICA and Myc-HMMR for 30 h. CHICA complexes were immunoprecipitated using sheep anti-GFP antibodies, and then Western blotted using mouse anti-GFP or mouse anti-Myc.

Downloaded from http://rupress.org/jcb/article-pdf/198/6/1039/1575829/jcb_201202112.pdf by guest on 09 February 2026

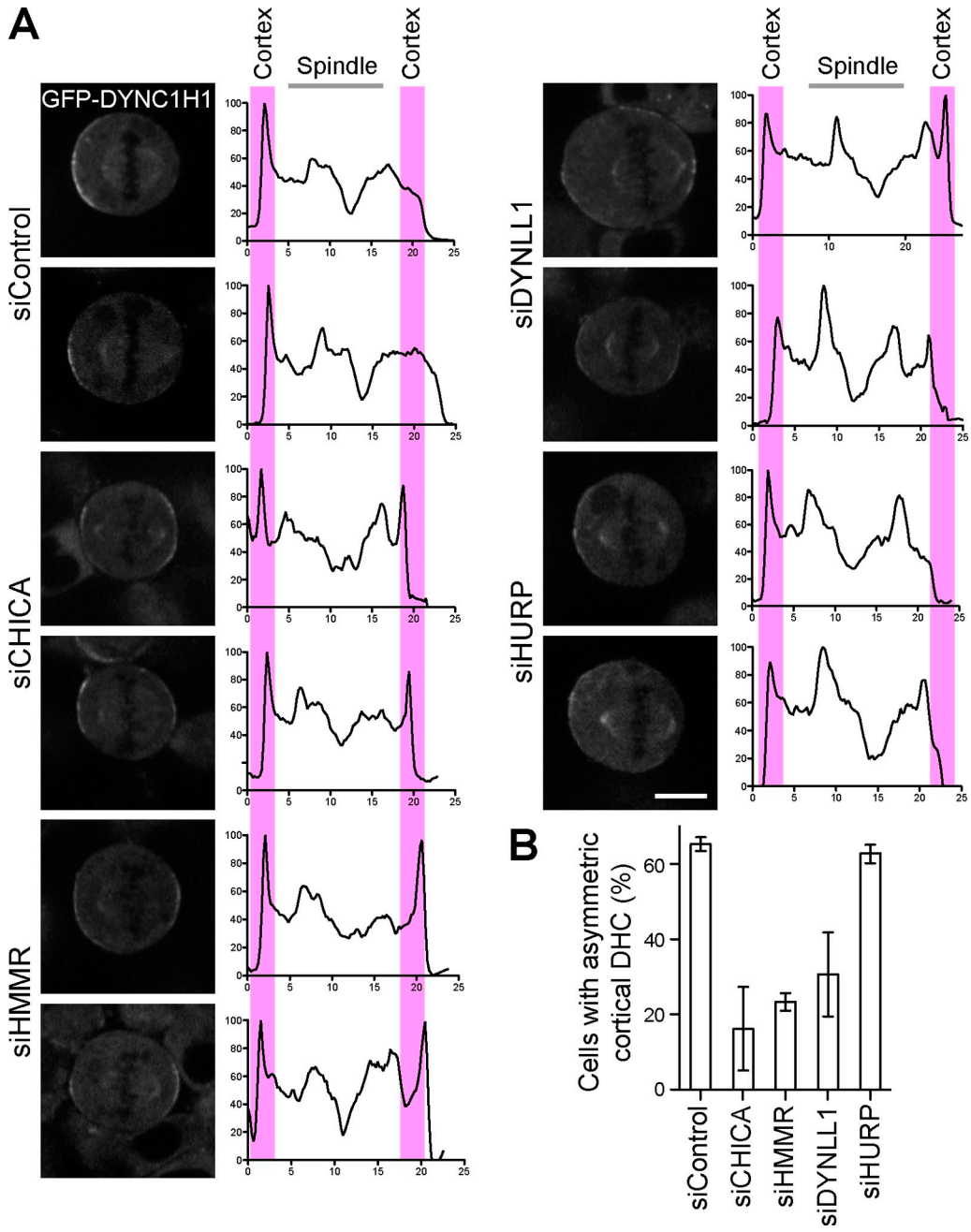

Figure 9. **Dynein heavy chain asymmetry is lost in DYNLL1-, CHICA-, and HMMR-depleted cells.** (A) GFP-dynein heavy chain (DYNC1H1) cells were transfected with control, CHICA, HMMR, DYNLL1, and HURP siRNA duplexes for 72 h. The cells were then imaged using an Ultraview Vox spinning-disk confocal system. Images of metaphase cells were taken from a single z-plane at one time point. Exposure times were 100 msec for GFP-DYNC1H1 using 50% laser power. Graphs representing the intensity profiles were generated with NIH ImageJ. A profile plot was made from a selection of 20 pixels width crossing the mitotic spindle at both spindle poles. Intensity values were extracted. An average background value was subtracted and values were normalized to the brightest point corresponding to 100%. Two representative example images and associated graphs are shown. Bar, 10 µm. (B) The cortical localization of dynein was scored in the different conditions used and is plotted in the bar graph. Error bars show the SEM (n = 25 in each of three independent experiments.

Materials and methods

Reagents and antibodies

General laboratory chemicals were obtained from Sigma-Aldrich and Thermo Fisher Scientific. Hexahistidine-tagged HMMR aa 183–364, CHICA-N aa 1–281, and HURP aa 673–890 were expressed in and purified from bacteria. Antibodies against HMMR, CHICA-N, and HURP were raised in sheep (Scottish National Blood Transfusion Service, Edinburgh, UK) and affinity purified using the His-tagged proteins coupled to Affigel-15 (Bio-Rad Laboratories). The CHICA-C antibody was raised in sheep using the CHICA peptide (CSRVNLLAVRD) as the antigen. The crude serum was affinity purified using the CHICA peptide coupled to Sulfo-link (Thermo Fisher Scientific). Commercial mouse monoclonal antibodies were used against α-tubulin (clone DM1A; Sigma-Aldrich), Bub1 (Abcam), dynein heavy chain and dynein intermediate chain (Sigma-Aldrich), HMMR (Abcam), Myc (clone 9E10; Sigma-Aldrich), and p150^{Glued} (BD); rabbit antibodies against astrin (Thein et al., 2007), CenpE (Bethyl Laboratories, Inc.), NuMA and pericentrin (Abcam), DYNLL1 (Epitomics, Inc.), KID (Cytoskeleton), Myc (Sigma-Aldrich), and TACC3 (Santa Cruz Biotechnology, Inc.); and sheep antibodies against Eg5 (Zeng et al., 2010), GFP

Downloaded from http://rupress.org/jcb/article-pdf/198/6/1039/1575829/jcb_201202112.pdf by guest on 09 February 2026

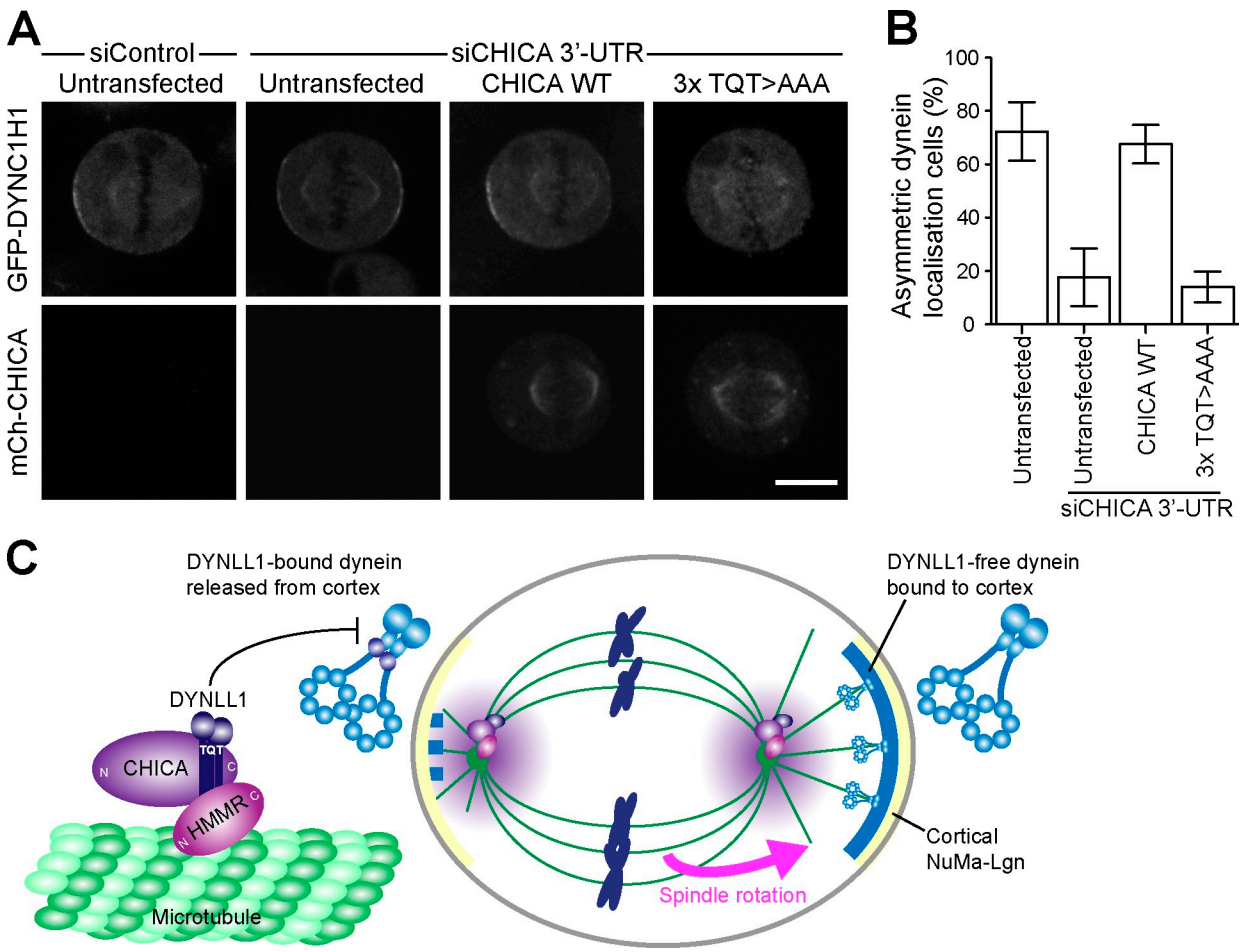

Figure 10. **Dynein heavy chain asymmetry is lost in DYNLL1-, CHICA-, and HMMR-depleted cells.** (A) GFP-dynein heavy chain (DYNC1H1) cells were transfected with control or CHICA 3′-UTR siRNA duplexes for 24 h, then left untransfected or further transfected with CHICA wild-type or the TQT mutant form for a further 48 h. The cells were then imaged using an Ultraview Vox spinning-disk confocal system. Images of metaphase cells were taken from a single z-plane at one time point. Exposure times were 100 msec for GFP-DYNC1H1 or mCherry-tagged CHICA using 50 or 30% laser power, respectively. (B) The cortical localization of dynein was scored and is plotted in the bar graph. Error bars show the SEM (n = 10 in each of two independent experiments). (C) A model or DYNLL1 function in spindle positioning and orientation. DYNLL1 is recruited to spindle poles by the triple TQT motifs in the CHICA-HMMR complex. HMMR contains an N-terminal microtubule-binding domain capable of targeting the complex to spindle microtubules. Because loss of DYNLL1 results in additional dynein at the cortex and DYNLL1 does not accumulate at the cell cortex, this model proposes that DYNLL1 is inhibitory to dynein targeting to the cortex. When a spindle pole carrying the DYNLL1–CHICA–HMMR complex approaches the cortex, this results in increased local concentration of DYNLL1 and removal of dynein from the cell cortex. Ultimately, this leads to a reduction in pulling forces on the mitotic spindle, which then fails to rotate to the correct position in response to extrinsic positioning cues.

(Shorter et al., 1999), and kinastrin (Dunsch et al., 2011). Kinetochores were visualized with CREST (human auto-antiserum; Europa Bioproducts Ltd.). Affinity-purified primary and secondary antibodies were used at 1 µg/ml final concentration; sera were used at 1:1,000 dilution. Secondary antibodies conjugated to HRP or Cy5 were obtained from Jackson ImmunoResearch Laboratories, Inc. Secondary antibodies conjugated to Alexa Fluor 488, 555, and 647 were obtained from Invitrogen. DNA was stained with DAPI (Sigma-Aldrich).

Molecular biology

Human CHICA, DYNLL1, HMMR, and EB1 were amplified from human testis cDNA (Takara Bio Inc.) using *KOD* polymerase (Takara Bio Inc.). Mammalian expression constructs for CHICA, DYNLL1, HMMR, and EB1 were made using pcDNA3.1, pcDNA4/TO, and pcDNA5/FRT/TO vectors (Invitrogen) modified to encode the Myc epitope tag, mCherry, or GFP reading frames. Bacterial expression constructs were made in pQE32 (QIAGEN). Mutagenesis was performed using the QuikChange method according to the protocol (Agilent Technologies). RNA interference for astrin, kinastrin, CenpE, GL2 luciferase (control), HURP, and Nuf2 was carried out using published (Dunsch et al., 2011) commercially available siRNA duplexes. Other siRNA duplexes were as follows: CHICA-1 5′-CAAUUCCACUUCGCUGGUAdTdT-3′; CHICA-2 5′-GAACUAAGAUUAUUGGGAAdTdT-3′; CHICA-3 5′-CCAGGATAGCAAGCTCTCAAA-3′; CHICA-4 5′-ATGGACGGATGGCAAATTAAA-3′; HMMR-1 5′-CUGAUUUGCAGAACCAACUdTdT-3′; HMMR-2 5′-GGAGAAUAUUGUUAUAUUAdTdT-3′; DYNNL1 Dharmacon SmartPool L-005281-00 (Thermo Fisher Scientific) or 5′-GAAGGACAUUGCGGCUCAUUU-3′; CHICA 3′-UTR 5′-GGTTTAAACACTATGGATA-3′; and TACC3 5′-GTTACCGGAAGATCGTCTG-3′.

Cell culture

HeLa cells and HEK293T were cultured in DME containing 10% bovine calf serum (Invitrogen) at 37°C and 5% CO_2. For synchronization, cells were treated for 18 h with 2 mM thymidine, washed three times in PBS, and twice with growth medium. For plasmid transfection and siRNA transfection, Mirus LT1 (Mirus Bio LLC) and Oligofectamine (Invitrogen), respectively, were used according to the manufacturers' instructions. Stable HeLa cell lines with single copies of the desired transgene were created using the T-Rex doxycycline-inducible Flp-In system (Invitrogen). HeLa cell lines stably expressing GFP-tagged α-tubulin selected using 0.5 µg/ml puromycin and mCherry-tagged histone H2B selected using 0.3 µg/ml blasticidin have been described previously (Zeng et al., 2010). The tagged transgenes and selection markers were under the control of the chicken β-actin promoter. Cell lines expressing GFP-tagged DYNC1H1 were obtained from the Mitocheck consortium (www.mitocheck.org).

Downloaded from http://rupress.org/jcb/article-pdf/198/6/1039/1575829/jcb_201202112.pdf by guest on 09 February 2026

Isolation of protein complexes

For immunoprecipitations of endogenous CHICA, DYNLL1, HMMR, or HURP, three 15-cm dishes of synchronized HeLa S3 cells per condition were released from the thymidine arrest for 3 h at 37°C, 100 ng/ml nocodazole was added, and the cells were incubated for a further 16 h. For HMMR or CHICA fragments, one 15-cm dish of HEK293T cells per condition was transfected with the appropriate construct for 30 h. Mitotic cells were collected by shake-off and nocodazole was removed by washing three times with prewarmed PBS and twice with growth medium. For metaphase samples, cells were collected and washed three times with ice-cold PBS. Cell pellets were resuspended in lysis buffer (20 mM Tris-HCl, pH 7.4, 150 mM NaCl, 1 mM EDTA, 1% [vol/vol] IGEPAL, 0.1% [wt/vol] sodium deoxycholate, 40 mM β-glycerophosphate, 10 mM NaF, 0.3 mM Na-vanadate, 100 nM okadaic acid, and protease inhibitor cocktail [SigmaAldrich]), left for 15 min on ice, and then clarified by centrifugation at 20,000 *g* for 15 min at 4°C. Protein complexes were isolated from 3 mg of cell lysate using 2.5 µg sheep antibodies against either mCherry, GFP, HMMR, or CHICA bound to 20 µl protein G–Sepharose by incubation for 3 h at 4°C. Isolated complexes were washed three times with lysis buffer, twice with 20 mM Tris-HCl, pH 7.4, 150 mM NaCl, 0.1% [vol/vol] IGEPAL, and then twice with 20 mM Tris-HCl, pH 7.4, 150 mM NaCl.

Mass spectrometry of protein complexes

Protein samples for mass spectrometry were separated on 4–12% gradient NuPAGE gels, then stained using a colloidal Coomassie blue stain. Gel lanes were cut into 12 slices, and then digested with trypsin (Wilm et al., 1996). The resulting tryptic peptide mixtures in 0.05% [vol/vol] trifluoracetic acid were then analyzed by online LC-MS/MS with a nanoAcquity UPLC (Waters) and an Orbitrap XL ETD mass spectrometer (Thermo Fisher Scientific) fitted with a Proxeon nano-electrospray source. Peptides were loaded on to a 5-cm × 180-µm BEH-C18 Symmetry trap column (part no. 186003514; Waters) in 0.1% [vol/vol] formic acid at 15 µl/min, and then resolved using a 25-cm × 75-µm BEH-C18 column (part no. 186003815; Waters) in 99–37.5% [vol/vol] acetonitrile in 0.1% [vol/vol] formic acid at a flow rate of 400 nl/min. The mass spectrometer was set to acquire an MS survey scan in the Orbitrap (R = 30,000) and then perform MS/MS on the top five ions in the linear quadrupole ion trap after fragmentation using collision ionization (30 msec, 35% energy). A 90-s rolling exclusion list with $n = 3$ was used to prevent redundant analysis of the same ions. Maxquant and Mascot (Matrix Science) were then used to compile and search the raw data against the human IPI database (Cox and Mann, 2008). Protein group and peptide lists were sorted and analyzed in Excel (Microsoft) and Maxquant. MS and MS/MS spectra were manually inspected using Xcalibur Qualbrowser (Thermo Fisher Scientific).

Fixed cell microscopy

Cells grown on no. 1.5 glass coverslips (Menzel-Gläser; Thermo Fisher Scientific) were washed twice with 2 ml of PBS, and fixed with 2 ml of 3% [wt/vol] paraformaldehyde in PBS for 15 min. Fixative was removed and the cells quenched with 2 ml of 50 mM NH_4Cl in PBS for 10 min. Coverslips were washed three times in 2 ml PBS before permeabilization in 0.2% [vol/vol] Triton X-100 for 10 min. In all cases primary and secondary antibody staining was performed in PBS for 60 min at room temperature. Affinity-purified antibodies were used at 1 µg/ml, whereas commercial antibodies were used as directed by the manufacturers. DAPI was added to the secondary antibody–staining solution at 1 µg/ml. Coverslips were mounted in Mowiol 4-88 mounting medium. Fixed samples on glass slides were imaged using a 60×, NA 1.35 oil immersion objective on an upright microscope (model BX61; Olympus) with filtersets for DAPI, GFP/Alexa Fluor 488, -555, -568, and -647 (Chroma Technology Corp.), a CoolSNAP HQ2 camera (Roper Scientific), and MetaMorph 7.5 imaging software (Molecular Dynamics Inc.). Illumination was provided by a Lumen 200 Watt metal halide light source (Prior Scientific Instruments Ltd.). Image stacks of 12–35 planes with a spacing of 0.2–0.4 µm through the cell volume were taken. Using MetaMorph, image stacks were maximum intensity projected and then merged to create 24-bit RGB TIFF files. Images in Figs. 2, 3, S2, and S3 were deconvolved using the nearest-neighbors method in MetaMorph. Images in 24-bit RGB format were then cropped in Photoshop CS3 and placed into Illustrator CS3 (Adobe Systems Inc.) to produce the figures.

Super-resolution imaging

3D structured illumination microscopy (3D-SIM) was performed as described previously (Schermelleh et al., 2008) on a DeltaVision OMX V2 system (Applied Precision) equipped with a 100× 1.4 NA oil immersion objective (Olympus) and Cascade II:512 EMCCD cameras (Roper Scientific), using the 405- and 488-nm diode laser lines. Cells for 3D-SIM were prepared as described for standard fixed cell microscopy with the following changes. The cells were grown on no. 1.5H precision glass coverslips (Marienfeld), then washed twice with 2 ml of PBS, and fixed with 2 ml of 4% [wt/vol] paraformaldehyde in PBS for 15 min. Coverslips were mounted in Vectashield mounting medium. Immersion oil with a refractive index of 1.514 was used after being empirically determined to give the most symmetric point spread function for the specific sample conditions. Image stacks (z-height of up to 18 µm, z-distance of 0.125) of the green (Alexa Fluor 488) and the blue (DAPI) fluorescence were recorded sequentially through the same emission light path. Exploiting the broad emission range of DAPI, this approach has the advantage to reduce additional bleaching of the green dye by otherwise interposed 405-nm excitation and avoids the need for post-acquisition channel alignment. Reconstruction was performed with the SoftWoRx 3.7 image-processing software (Applied Precision) to obtain a super-resolution 3D image stack with an optical resolution of 120 nm in the lateral, and approximately 300 nm in the axial direction. These 3D image stacks were imported into Volocity, and a maximum-intensity projection performed. These 24-bit RGB TIFF format images were placed into Illustrator CS3 (Adobe Systems Inc.) to produce the figures.

Live-cell microscopy

For live-cell imaging, cells were plated in 35-mm dishes with a 14-mm no. 1.5 thickness coverglass window in the bottom (MatTek Corporation). For imaging, the dishes were placed in a 37°C and 5% CO_2 environment chamber (Tokai Hit) on the microscope stage. Imaging was performed at 37°C in 5% CO_2 using an inverted microscope (model IX81; Olympus) with a 60× 1.42 NA oil immersion objective coupled to a spinning-disk confocal system (Ultraview Vox; PerkinElmer) fitted with an EM-CCD camera (model C9100-13; Hamamatsu Photonics). Exposure times were 30 msec for GFP-tubulin or mCherry-tagged histone H2B using 4% laser power, 100 msec and 30% laser power for mCherry-EB1, and 100 msec and 50% laser power for dynein heavy chain-GFP. For tubulin and histone double stable cells, image stacks of 29 planes spaced 0.6 µm apart were taken at 1–4 stage positions every minute for up to 12 h. For experiments analyzing EB1, 7 planes spaced 0.4 µm apart were captured at the maximum rate. Due to the low signal intensity only a single plane was captured for dynein heavy chain. Maximum intensity projection of the fluorescent channels was performed in Volocity to create 24-bit RGB TIFF files. Images in 24-bit RGB TIFF format were then placed into Adobe Illustrator CS3 to produce the figures.

Microtubule-binding assays

Full-length protein and fragments of CHICA, HMMR, Rab4, and PRC1 were in vitro translated (IVT) and labeled with ^{35}S-methionine using the TnT Coupled Reticulocyte Lysate System (Promega) according to the manufacturer's recommendations. Microtubules were prepared from bovine brain tubulin (20 µl, 5 mg/ml; Cytoskeleton) by incubation with 200 µl PEM buffer (80 mM Pipes, pH 7.0, 0.5 mM EGTA, and 2 mM $MgCl_2$), 2 µl of cushion buffer (60% [vol/vol] glycerol, 80 mM Pipes, pH 7.0, 1 mM EGTA, 1 mM MgCl), 0.22 µl 100 mM GTP, and 2 µl of 2 mM paclitaxel for 20 min at 35°C. All following procedures were performed at room temperature, ∼22–24°C. A 3-µl aliquot of the IVT mix was diluted in PEM buffer supplemented with 0.1% [vol/vol] Triton X-100, 0.5 mg/ml BSA, and 50 mM NaCl in a final volume of 50 µl. The reaction mixture was clarified by centrifugation at 90,000 rpm for 10 min in a TLA-100.3 rotor (Beckman Coulter). This clarified IVT fraction was incubated with 20 µl of taxol-stabilized microtubules for 10 min. The reactions were layered over 100 µl of cushion buffer and centrifuged at 80,000 rpm for 10 min at room temperature in the TLA-100.3 rotor.

Online supplemental material

Fig. S1 shows characterization of new CHICA and HMMR antibodies and siRNA duplexes. Fig. S2 shows the analysis of kinetochore fibers stability and checkpoint function. Fig. S3 describes the localization of NuMA and Plk1 when DYNLL1, CHICA, or HMMR are depleted. Videos 1–4 accompany Fig. 4 and show the effects of DYNLL1, CHICA, or HMMR depletion on spindle formation and position. Video 5 shows a rotation of mitotic spindles in CHICA-depleted cells. Microtubule dynamics were tracked using EB1, and these movies accompanying Fig. 6 D are shown in Videos 6–10. Table S1 shows the mass spectrometry data identifying the proteins in DYNLL1 and CHICA complexes. Online supplemental material is available at http://www.jcb.org/cgi/content/full/jcb.201202112/DC1.

We thank Ricardo Nunes Bastos and Kang Zeng for reagents and advice during the course of this work, Emily Linnane for initial help with GFP-DYNLL1 cell lines, and Ian Dobbie (Micron Advanced Bioimaging Unit) for technical help.

Downloaded from http://rupress.org/jcb/article-pdf/198/6/1039/1575829/jcb_201202112.pdf by guest on 09 February 2026

This work was supported by a Cancer Research UK program grant to F.A. Barr (C20079/A9473). A.K. Dunsch holds a Boehringer Ingelheim Fonds PhD fellowship. The work of L. Schermelleh and the Micron Advanced Bioimaging Unit was funded by the Wellcome Trust (067413).

Submitted: 21 February 2012
Accepted: 20 August 2012

References

Bowman, S.K., R.A. Neumüller, M. Novatchkova, Q. Du, and J.A. Knoblich. 2006. The *Drosophila* NuMA Homolog Mud regulates spindle orientation in asymmetric cell division. *Dev. Cell*. 10:731–742. http://dx.doi.org/10.1016/j.devcel.2006.05.005

Busson, S., D. Dujardin, A. Moreau, J. Dompierre, and J.R. De Mey. 1998. Dynein and dynactin are localized to astral microtubules and at cortical sites in mitotic epithelial cells. *Curr. Biol.* 8:541–544. http://dx.doi.org/10.1016/S0960-9822(98)70208-8

Buttrick, G.J., L.M. Beaumont, J. Leitch, C. Yau, J.R. Hughes, and J.G. Wakefield. 2008. Akt regulates centrosome migration and spindle orientation in the early *Drosophila melanogaster* embryo. *J. Cell Biol.* 180:537–548. http://dx.doi.org/10.1083/jcb.200705085

Cabernard, C., and C.Q. Doe. 2009. Apical/basal spindle orientation is required for neuroblast homeostasis and neuronal differentiation in *Drosophila*. *Dev. Cell*. 17:134–141. http://dx.doi.org/10.1016/j.devcel.2009.06.009

Chan, Y.W., L.L. Fava, A. Uldschmid, M.H. Schmitz, D.W. Gerlich, E.A. Nigg, and A. Santamaria. 2009. Mitotic control of kinetochore-associated dynein and spindle orientation by human Spindly. *J. Cell Biol.* 185: 859–874. http://dx.doi.org/10.1083/jcb.200812167

Cockell, M.M., K. Baumer, and P. Gönczy. 2004. lis-1 is required for dynein-dependent cell division processes in *C. elegans* embryos. *J. Cell Sci.* 117:4571–4582. http://dx.doi.org/10.1242/jcs.01344

Cox, J., and M. Mann. 2008. MaxQuant enables high peptide identification rates, individualized p.p.b.-range mass accuracies and proteome-wide protein quantification. *Nat. Biotechnol.* 26:1367–1372. http://dx.doi.org/10.1038/nbt.1511

Dunsch, A.K., E. Linnane, F.A. Barr, and U. Gruneberg. 2011. The astrin-kinastrin/SKAP complex localizes to microtubule plus ends and facilitates chromosome alignment. *J. Cell Biol.* 192:959–968. http://dx.doi.org/10.1083/jcb.201008023

Echeverri, C.J., B.M. Paschal, K.T. Vaughan, and R.B. Vallee. 1996. Molecular characterization of the 50-kD subunit of dynactin reveals function for the complex in chromosome alignment and spindle organization during mitosis. *J. Cell Biol.* 132:617–633. http://dx.doi.org/10.1083/jcb.132.4.617

Ellefson, M.L., and F.J. McNally. 2011. CDK-1 inhibits meiotic spindle shortening and dynein-dependent spindle rotation in *C. elegans*. *J. Cell Biol.* 193:1229–1244. http://dx.doi.org/10.1083/jcb.201104008

Evanko, S.P., W.T. Parks, and T.N. Wight. 2004. Intracellular hyaluronan in arterial smooth muscle cells: association with microtubules, RHAMM, and the mitotic spindle. *J. Histochem. Cytochem.* 52:1525–1535. http://dx.doi.org/10.1369/jhc.4A6356.2004

Faulkner, N.E., D.L. Dujardin, C.Y. Tai, K.T. Vaughan, C.B. O'Connell, Y. Wang, and R.B. Vallee. 2000. A role for the lissencephaly gene LIS1 in mitosis and cytoplasmic dynein function. *Nat. Cell Biol.* 2:784–791. http://dx.doi.org/10.1038/35041020

Fernández-Miñán, A., M.D. Martín-Bermudo, and A. González-Reyes. 2007. Integrin signaling regulates spindle orientation in *Drosophila* to preserve the follicular-epithelium monolayer. *Curr. Biol.* 17:683–688. http://dx.doi.org/10.1016/j.cub.2007.02.052

Fink, J., N. Carpi, T. Betz, A. Bétard, M. Chebah, A. Azioune, M. Bornens, C. Sykes, L. Fetler, D. Cuvelier, and M. Piel. 2011. External forces control mitotic spindle positioning. *Nat. Cell Biol.* 13:771–778. http://dx.doi.org/10.1038/ncb2269

Gassmann, R., A.J. Holland, D. Varma, X. Wan, F. Civril, D.W. Cleveland, K. Oegema, E.D. Salmon, and A. Desai. 2010. Removal of Spindly from microtubule-attached kinetochores controls spindle checkpoint silencing in human cells. *Genes Dev.* 24:957–971. http://dx.doi.org/10.1101/gad.1886810

Gönczy, P., S. Pichler, M. Kirkham, and A.A. Hyman. 1999. Cytoplasmic dynein is required for distinct aspects of MTOC positioning, including centrosome separation, in the one cell stage *Caenorhabditis elegans* embryo. *J. Cell Biol.* 147:135–150. http://dx.doi.org/10.1083/jcb.147.1.135

Gotta, M., M.C. Abraham, and J. Ahringer. 2001. CDC-42 controls early cell polarity and spindle orientation in *C. elegans*. *Curr. Biol.* 11:482–488. http://dx.doi.org/10.1016/S0960-9822(01)00142-7

Groen, A.C., L.A. Cameron, M. Coughlin, D.T. Miyamoto, T.J. Mitchison, and R. Ohi. 2004. XRHAMM functions in ran-dependent microtubule nucleation and pole formation during anastral spindle assembly. *Curr. Biol.* 14:1801–1811. http://dx.doi.org/10.1016/j.cub.2004.10.002

Inaba, M., H. Yuan, V. Salzmann, M.T. Fuller, and Y.M. Yamashita. 2010. E-cadherin is required for centrosome and spindle orientation in *Drosophila* male germline stem cells. *PLoS ONE*. 5:e12473. http://dx.doi.org/10.1371/journal.pone.0012473

Jaffe, A.B., N. Kaji, J. Durgan, and A. Hall. 2008. Cdc42 controls spindle orientation to position the apical surface during epithelial morphogenesis. *J. Cell Biol.* 183:625–633. http://dx.doi.org/10.1083/jcb.200807121

Johnston, C.A., K. Hirono, K.E. Prehoda, and C.Q. Doe. 2009. Identification of an Aurora-A/PinsLINKER/Dlg spindle orientation pathway using induced cell polarity in S2 cells. *Cell*. 138:1150–1163. http://dx.doi.org/10.1016/j.cell.2009.07.041

Kaltschmidt, J.A., C.M. Davidson, N.H. Brown, and A.H. Brand. 2000. Rotation and asymmetry of the mitotic spindle direct asymmetric cell division in the developing central nervous system. *Nat. Cell Biol.* 2:7–12. http://dx.doi.org/10.1038/71323

Kardon, J.R., and R.D. Vale. 2009. Regulators of the cytoplasmic dynein motor. *Nat. Rev. Mol. Cell Biol.* 10:854–865. http://dx.doi.org/10.1038/nrm2804

Kiyomitsu, T., and I.M. Cheeseman. 2012. Chromosome- and spindle-pole-derived signals generate an intrinsic code for spindle position and orientation. *Nat. Cell Biol.* 14:311–317. http://dx.doi.org/10.1038/ncb2440

Laan, L., N. Pavin, J. Husson, G. Romet-Lemonne, M. van Duijn, M.P. López, R.D. Vale, F. Jülicher, S.L. Reck-Peterson, and M. Dogterom. 2012. Cortical dynein controls microtubule dynamics to generate pulling forces that position microtubule asters. *Cell*. 148:502–514. http://dx.doi.org/10.1016/j.cell.2012.01.007

Li, Y.Y., E. Yeh, T. Hays, and K. Bloom. 1993. Disruption of mitotic spindle orientation in a yeast dynein mutant. *Proc. Natl. Acad. Sci. USA*. 90: 10096–10100. http://dx.doi.org/10.1073/pnas.90.21.10096

Lo, K.W., S. Naisbitt, J.S. Fan, M. Sheng, and M. Zhang. 2001. The 8-kDa dynein light chain binds to its targets via a conserved (K/R)XTQT motif. *J. Biol. Chem.* 276:14059–14066. http://dx.doi.org/10.1074/jbc.M104701200

Maxwell, C.A., J.J. Keats, M. Crainie, X. Sun, T. Yen, E. Shibuya, M. Hendzel, G. Chan, and L.M. Pilarski. 2003. RHAMM is a centrosomal protein that interacts with dynein and maintains spindle pole stability. *Mol. Biol. Cell*. 14:2262–2276. http://dx.doi.org/10.1091/mbc.E02-07-0377

McKenney, R.J., S.J. Weil, J. Scherer, and R.B. Vallee. 2011. Mutually exclusive cytoplasmic dynein regulation by NudE-Lis1 and dynactin. *J. Biol. Chem.* 286:39615–39622. http://dx.doi.org/10.1074/jbc.M111.289017

Mitsushima, M., F. Toyoshima, and E. Nishida. 2009. Dual role of Cdc42 in spindle orientation control of adherent cells. *Mol. Cell. Biol.* 29: 2816–2827. http://dx.doi.org/10.1128/MCB.01713-08

Morin, X., and Y. Bellaïche. 2011. Mitotic spindle orientation in asymmetric and symmetric cell divisions during animal development. *Dev. Cell*. 21: 102–119. http://dx.doi.org/10.1016/j.devcel.2011.06.012

Nguyen-Ngoc, T., K. Afshar, and P. Gönczy. 2007. Coupling of cortical dynein and G alpha proteins mediates spindle positioning in *Caenorhabditis elegans*. *Nat. Cell Biol.* 9:1294–1302. http://dx.doi.org/10.1038/ncb1649

O'Connell, C.B., and Y.L. Wang. 2000. Mammalian spindle orientation and position respond to changes in cell shape in a dynein-dependent fashion. *Mol. Biol. Cell*. 11:1765–1774.

Pfarr, C.M., M. Coue, P.M. Grissom, T.S. Hays, M.E. Porter, and J.R. McIntosh. 1990. Cytoplasmic dynein is localized to kinetochores during mitosis. *Nature*. 345:263–265. http://dx.doi.org/10.1038/345263a0

Poulson, N.D., and T. Lechler. 2010. Robust control of mitotic spindle orientation in the developing epidermis. *J. Cell Biol.* 191:915–922. http://dx.doi.org/10.1083/jcb.201008001

Qin, Y., W.H. Meisen, Y. Hao, and I.G. Macara. 2010. Tuba, a Cdc42 GEF, is required for polarized spindle orientation during epithelial cyst formation. *J. Cell Biol.* 189:661–669. http://dx.doi.org/10.1083/jcb.201002097

Rapali, P., L. Radnai, D. Süveges, V. Harmat, F. Tölgyesi, W.Y. Wahlgren, G. Katona, L. Nyitray, and G. Pál. 2011a. Directed evolution reveals the binding motif preference of the LC8/DYNLL hub protein and predicts large numbers of novel binders in the human proteome. *PLoS ONE*. 6:e18818. http://dx.doi.org/10.1371/journal.pone.0018818

Rapali, P., A. Szenes, L. Radnai, A. Bakos, G. Pál, and L. Nyitray. 2011b. DYNLL/LC8: a light chain subunit of the dynein motor complex and beyond. *FEBS J.* 278:2980–2996. http://dx.doi.org/10.1111/j.1742-4658.2011.08254.x

Rebollo, E., P. Sampaio, J. Januschke, S. Llamazares, H. Varmark, and C. González. 2007. Functionally unequal centrosomes drive spindle orientation in asymmetrically dividing *Drosophila* neural stem cells. *Dev. Cell*. 12:467–474. http://dx.doi.org/10.1016/j.devcel.2007.01.021

Downloaded from http://rupress.org/jcb/article-pdf/198/6/1039/1575829/jcb_201202112.pdf by guest on 09 February 2026

Rhyu, M.S., and J.A. Knoblich. 1995. Spindle orientation and asymmetric cell fate. *Cell*. 82:523–526. http://dx.doi.org/10.1016/0092-8674(95)90022-5

Rodriguez-Fraticelli, A.E., S. Vergarajauregui, D.J. Eastburn, A. Datta, M.A. Alonso, K. Mostov, and F. Martín-Belmonte. 2010. The Cdc42 GEF Intersectin 2 controls mitotic spindle orientation to form the lumen during epithelial morphogenesis. *J. Cell Biol.* 189:725–738. http://dx.doi.org/10.1083/jcb.201002047

Samora, C.P., B. Mogessie, L. Conway, J.L. Ross, A. Straube, and A.D. McAinsh. 2011. MAP4 and CLASP1 operate as a safety mechanism to maintain a stable spindle position in mitosis. *Nat. Cell Biol.* 13:1040–1050. http://dx.doi.org/10.1038/ncb2297

Sanada, K., and L.H. Tsai. 2005. G protein betagamma subunits and AGS3 control spindle orientation and asymmetric cell fate of cerebral cortical progenitors. *Cell*. 122:119–131. http://dx.doi.org/10.1016/j.cell.2005.05.009

Santamaria, A., S. Nagel, H.H. Sillje, and E.A. Nigg. 2008. The spindle protein CHICA mediates localization of the chromokinesin Kid to the mitotic spindle. *Curr. Biol.* 18:723–729. http://dx.doi.org/10.1016/j.cub.2008.04.041

Scaërou, F., I. Aguilera, R. Saunders, N. Kane, L. Blottière, and R. Karess. 1999. The rough deal protein is a new kinetochore component required for accurate chromosome segregation in *Drosophila*. *J. Cell Sci.* 112: 3757–3768.

Schermelleh, L., P.M. Carlton, S. Haase, L. Shao, L. Winoto, P. Kner, B. Burke, M.C. Cardoso, D.A. Agard, M.G.L. Gustafsson, et al. 2008. Subdiffraction multicolor imaging of the nuclear periphery with 3D structured illumination microscopy. *Science*. 320:1332–1336. http://dx.doi.org/10.1126/science.1156947

Schmidt, J.C., T. Kiyomitsu, T. Hori, C.B. Backer, T. Fukagawa, and I.M. Cheeseman. 2010. Aurora B kinase controls the targeting of the Astrin-SKAP complex to bioriented kinetochores. *J. Cell Biol.* 191:269–280. http://dx.doi.org/10.1083/jcb.201006129

Sharp, D.J., G.C. Rogers, and J.M. Scholey. 2000. Cytoplasmic dynein is required for poleward chromosome movement during mitosis in *Drosophila* embryos. *Nat. Cell Biol.* 2:922–930. http://dx.doi.org/10.1038/35046574

Shorter, J., R. Watson, M.E. Giannakou, M. Clarke, G. Warren, and F.A. Barr. 1999. GRASP55, a second mammalian GRASP protein involved in the stacking of Golgi cisternae in a cell-free system. *EMBO J.* 18:4949–4960. http://dx.doi.org/10.1093/emboj/18.18.4949

Siller, K.H., and C.Q. Doe. 2009. Spindle orientation during asymmetric cell division. *Nat. Cell Biol.* 11:365–374. http://dx.doi.org/10.1038/ncb0409-365

Siller, K.H., C. Cabernard, and C.Q. Doe. 2006. The NuMA-related Mud protein binds Pins and regulates spindle orientation in *Drosophila* neuroblasts. *Nat. Cell Biol.* 8:594–600. http://dx.doi.org/10.1038/ncb1412

Starr, D.A., B.C. Williams, T.S. Hays, and M.L. Goldberg. 1998. ZW10 helps recruit dynactin and dynein to the kinetochore. *J. Cell Biol.* 142:763–774. http://dx.doi.org/10.1083/jcb.142.3.763

Stehman, S.A., Y. Chen, R.J. McKenney, and R.B. Vallee. 2007. NudE and NudEL are required for mitotic progression and are involved in dynein recruitment to kinetochores. *J. Cell Biol.* 178:583–594. http://dx.doi.org/10.1083/jcb.200610112

Steuer, E.R., L. Wordeman, T.A. Schroer, and M.P. Sheetz. 1990. Localization of cytoplasmic dynein to mitotic spindles and kinetochores. *Nature*. 345:266–268. http://dx.doi.org/10.1038/345266a0

Thein, K.H., J. Kleylein-Sohn, E.A. Nigg, and U. Gruneberg. 2007. Astrin is required for the maintenance of sister chromatid cohesion and centrosome integrity. *J. Cell Biol.* 178:345–354. http://dx.doi.org/10.1083/jcb.200701163

Théry, M., V. Racine, A. Pépin, M. Piel, Y. Chen, J.B. Sibarita, and M. Bornens. 2005. The extracellular matrix guides the orientation of the cell division axis. *Nat. Cell Biol.* 7:947–953. http://dx.doi.org/10.1038/ncb1307

Théry, M., A. Jiménez-Dalmaroni, V. Racine, M. Bornens, and F. Jülicher. 2007. Experimental and theoretical study of mitotic spindle orientation. *Nature*. 447:493–496. http://dx.doi.org/10.1038/nature05786

Tolg, C., S.R. Hamilton, L. Morningstar, J. Zhang, S. Zhang, K.V. Esguerra, P.G. Telmer, L.G. Luyt, R. Harrison, J.B. McCarthy, and E.A. Turley. 2010. RHAMM promotes interphase microtubule instability and mitotic spindle integrity through MEK1/ERK1/2 activity. *J. Biol. Chem.* 285: 26461–26474. http://dx.doi.org/10.1074/jbc.M110.121491

Toyoshima, F., and E. Nishida. 2007. Integrin-mediated adhesion orients the spindle parallel to the substratum in an EB1- and myosin X-dependent manner. *EMBO J.* 26:1487–1498. http://dx.doi.org/10.1038/sj.emboj.7601599

Toyoshima, F., S. Matsumura, H. Morimoto, M. Mitsushima, and E. Nishida. 2007. PtdIns(3,4,5)P3 regulates spindle orientation in adherent cells. *Dev. Cell*. 13:796–811. http://dx.doi.org/10.1016/j.devcel.2007.10.014

van der Voet, M., C.W. Berends, A. Perreault, T. Nguyen-Ngoc, P. Gönczy, M. Vidal, M. Boxem, and S. van den Heuvel. 2009. NuMA-related LIN-5, ASPM-1, calmodulin and dynein promote meiotic spindle rotation independently of cortical LIN-5/GPR/Galpha. *Nat. Cell Biol.* 11:269–277. http://dx.doi.org/10.1038/ncb1834

Vaughan, K.T., E.L. Holzbaur, and R.B. Vallee. 1995. Subcellular targeting of the retrograde motor cytoplasmic dynein. *Biochem. Soc. Trans.* 23:50–54.

Williams, B.C., Z. Li, S. Liu, E.V. Williams, G. Leung, T.J. Yen, and M.L. Goldberg. 2003. Zwilch, a new component of the ZW10/ROD complex required for kinetochore functions. *Mol. Biol. Cell*. 14:1379–1391. http://dx.doi.org/10.1091/mbc.E02-09-0624

Wilm, M., A. Shevchenko, T. Houthaeve, S. Breit, L. Schweigerer, T. Fotsis, and M. Mann. 1996. Femtomole sequencing of proteins from polyacrylamide gels by nano-electrospray mass spectrometry. *Nature*. 379:466–469. http://dx.doi.org/10.1038/379466a0

Wojcik, E., R. Basto, M. Serr, F. Scaërou, R. Karess, and T. Hays. 2001. Kinetochore dynein: its dynamics and role in the transport of the Rough deal checkpoint protein. *Nat. Cell Biol.* 3:1001–1007. http://dx.doi.org/10.1038/ncb1101-1001

Woodard, G.E., N.N. Huang, H. Cho, T. Miki, G.G. Tall, and J.H. Kehrl. 2010. Ric-8A and Gi alpha recruit LGN, NuMA, and dynein to the cell cortex to help orient the mitotic spindle. *Mol. Cell. Biol.* 30:3519–3530. http://dx.doi.org/10.1128/MCB.00394-10

Zeng, K., R.N. Bastos, F.A. Barr, and U. Gruneberg. 2010. Protein phosphatase 6 regulates mitotic spindle formation by controlling the T-loop phosphorylation state of Aurora A bound to its activator TPX2. *J. Cell Biol.* 191:1315–1332. http://dx.doi.org/10.1083/jcb.201008106

Zheng, Z., H. Zhu, Q. Wan, J. Liu, Z. Xiao, D.P. Siderovski, and Q. Du. 2010. LGN regulates mitotic spindle orientation during epithelial morphogenesis. *J. Cell Biol.* 189:275–288. http://dx.doi.org/10.1083/jcb.200910021

Downloaded from http://rupress.org/jcb/article-pdf/198/6/1039/1575829/jcb_201202112.pdf by guest on 09 February 2026